



1
2
3
4
5
6
7
8
9
10
11
12
13
14
15
16
17
18
19
20
21
22
23
24
25
26
27
28
29
30
31

Water Resources Research

Stable and Radioisotope Systematics Reveal Fossil Water as Fundamental Characteristic of Arid Orogenic-Scale Groundwater Systems

Brendan J. Moran (ORCID = 0000-0002-9862-6241)¹, David F. Boutt (ORCID = 0000-0003-1397-0279)¹, Lee Ann Munk (ORCID =0000-0003-2850-545X)²

¹ Department of Geosciences, University of Massachusetts-Amherst, Amherst, MA, USA

² Department of Geological Sciences, 3101 Science Circle, University of Alaska-Anchorage, Anchorage, AK, USA

Corresponding author: Brendan J. Moran (bmoran@geo.umass.edu)

Key points

- Tritium analysis shows shallow inflow waters to Salar de Atacama basin are composed predominantly of recharge greater than 60 years old.
- Inflow waters to Salar de Atacama are distinctly heterogeneous and decoupled from recharge on the Altiplano-Puna plateau.
- Stable water isotope analysis of 900 samples constrains the spatiotemporal dimensions of modern and fossil groundwaters in the Central Andes.

Keywords: Salar de Atacama, Chile, paleo-recharge, Tritium, Altiplano-Puna plateau, regional groundwater flow

Abstract

32 In arid and semi-arid regions, persistent hydrological imbalances illuminate the
33 considerable gaps in our spatiotemporal understating of fundamental catchment-scale governing
34 mechanisms. The Salar de Atacama basin (SdA) is the most extreme example of these
35 groundwater-dominated systems and as such is an ideal place to probe these unresolved
36 questions. Geochemical and hydrophysical observations indicate that groundwaters discharging to
37 the basin reflect a large regional system integrated over very long time-scales. The groundwater
38 here, as in other arid regions is a critical freshwater resource subject to substantial demand from
39 competing interests, particularly as development of its world-class lithium brine deposit expands.
40 Utilizing a uniquely large and comprehensive set of ^2H , ^{18}O and Tritium (^3H) tracer data we
41 demonstrate that much of the presumed recharge area on the Altiplano-Puna plateau exhibits
42 isotopic signatures quite distinct from waters presently discharging within the endorheic SdA
43 watershed. $\delta^{18}\text{O}$ values of predicted inflow source waters differ from modern plateau waters by
44 3.6‰ to 5.6‰ and ^3H data from 87 discrete samples indicate nearly all of this inflow is composed
45 of pre-modern recharge. Under plausible conditions, these distinctions cannot be explained solely
46 by natural variability in modern meteoric inputs or by steady-state groundwater flow. We present
47 a conceptual model revealing the extensive influence of transient draining of pre-modern
48 groundwater storage augmented by regional interbasin flow from the Andes. Our analysis
49 provides robust constraints on fundamental mechanisms governing this arid continental
50 groundwater system and a framework within which to address persistent uncertainties in these
51 systems worldwide.

52

53 **1. Introduction**

54 In the driest places on Earth, internally drained basins of various scales exhibit
55 groundwater discharge rates which exceed modern recharge (Gleeson et al., 2012; Scanlon et al.,
56 2006; Van Beek et al., 2011). These hydrologic budget imbalances have been observed or
57 inferred in nearly every arid region including: the southwestern United States (Belcher et al.,
58 2009; Kafri et al., 2012, Love et al., 2018; Wheatler et al., 2007), the Himalayan-Tibetan plateau
59 (Ge et al., 2016 and references therein), central Australia (Skrzypek et al., 2016; Wood et al.,
60 2015), the Sahara desert (Gasse et al, 2000; Kröpelin et al., 2008), the Arabian peninsula (Burg et
61 al. 2013; Müller et al., 2016; Wheatler et al., 2007) and the central Andes (Corenthal et al., 2016
62 and references therein). Difficulty constraining fundamental hydrological processes such as the
63 response times, flow paths and distribution and timing of groundwater recharge is magnified by
64 long residence times (>1 ka), deep water tables (>100 m) and often insufficient data (Favreau et
65 al., 2009; Gleeson et al., 2011; Walvoord et al., 2002). Uncertainties among inputs are

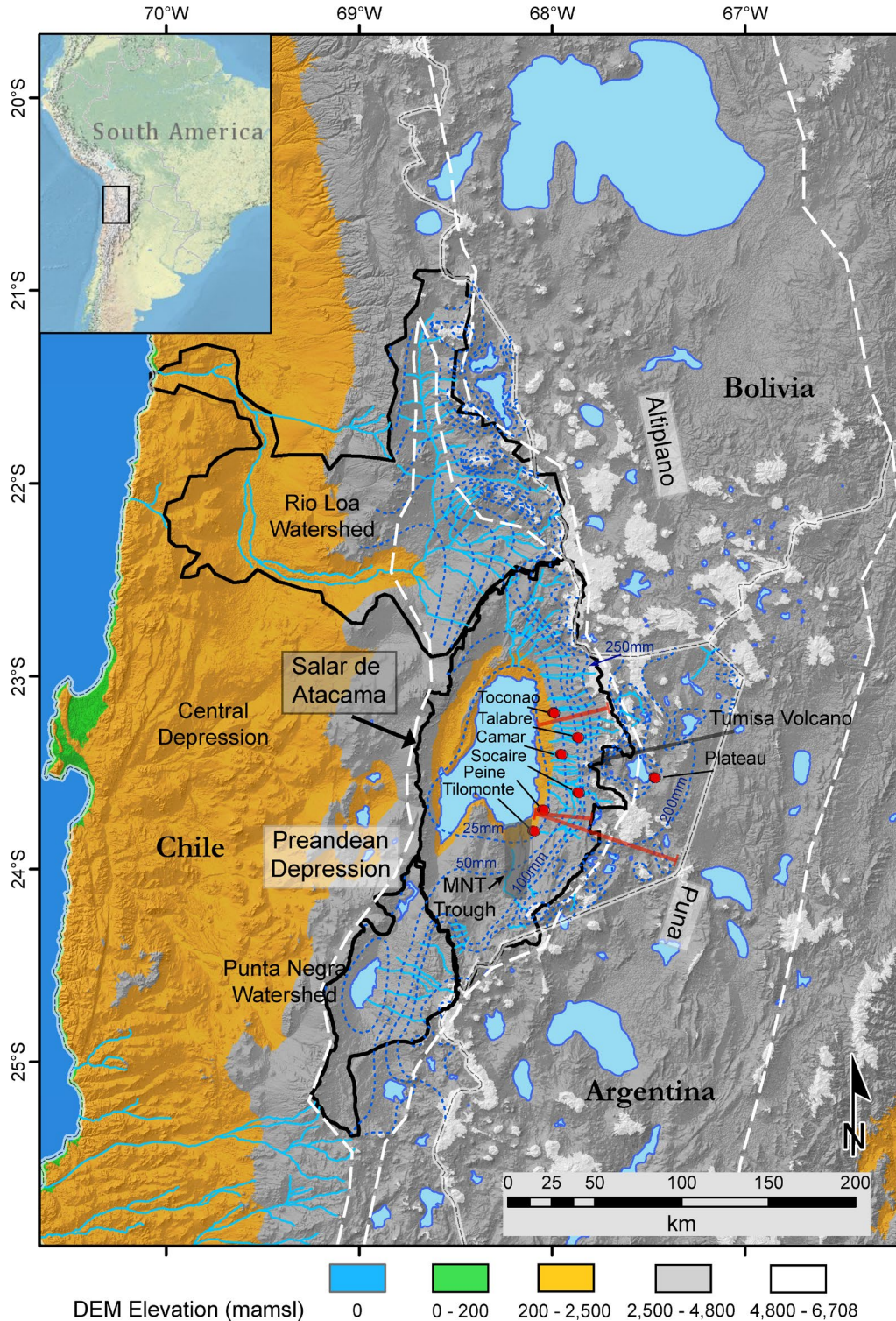


Figure 1. Shaded relief digital elevation model of the Central Andes. Salars, lagoons and major drainages (quebradas and rivers) are light blue. Topographic watersheds of major basins are outlined in black. Extent of the Preandean Depression and Altiplano/Puna plateau are outlined in white dashes. Isohyetal contours with associated values are dark blue dashed lines. Locations of generalized geologic cross-sections in Figure S1 are red. Red dots are precipitation gauges and sites used for HYSPLIT models. MNT Trough structure is shaded.

67 compounded by equally large uncertainties in discharge, which in these endorheic systems occurs
68 exclusively through evapotranspiration (Kampf & Tyler, 2006; Tyler et al., 1997). Fundamental
69 uncertainties have perpetuated inconsistencies in our conceptual models of system-wide
70 groundwater flow and the spatiotemporal dimensions of this flow, as a result it is clear that
71 current conceptual models need to be adjusted or altogether re-evaluated (e.g. Currell et al., 2016;
72 Haitjema & Mitchell-Bruker, 2005).

73 In the Preandean Depression, a large intramontane depression on the margin of the hyper-
74 arid core of the Atacama Desert and the Central Andean Plateau, it has been shown that water and
75 solute budgets are difficult to close under currently accepted spatiotemporal dimensions (Figure
76 1). In the Río Loa watershed to the north (i.e. the Calama Basin), anomalous water discharge
77 volumes have been observed (e.g., Jordan et al., 2015) and the Central Depression to the west has
78 anomalous nitrate accumulation (Pérez-Fodich et al., 2014). The most prominent feature in the
79 region, the Salar de Atacama basin (SdA) is defined by very large elevation and precipitation
80 gradients which have led to the development of an orogenic-scale groundwater system
81 encompassing portions of the adjacent Altiplano-Puna plateau. Recent work has concluded that
82 solute and water influx to SdA would need to be 9-20 times greater than modern to account for
83 the massive evaporite deposit accumulated there since the Miocene (Boutt et al., 2018; Corenthal
84 et al., 2016), but also that it is possible to accumulate the Li deposit from low temperature
85 weathering within a reasonable timeframe (Munk et al., 2018). Fundamental aspects of
86 subsurface fluid flow remain unresolved including: (i) catchment-wide response times to changes
87 in recharge and water tables, (ii) spatial and temporal connections between the modern and paleo-
88 hydrological systems, and (iii) the sources of additional water and solutes required to balance
89 mass at various scales. The SdA basin and its larger groundwater system is an ideal place to
90 methodically address these unresolved questions; this work advances our understanding of each.

91 The hydrogeologic system of SdA ranks as the most extreme on Earth; on the margin of
92 the driest non-polar desert and flanked by one of the highest and broadest plateaus. (Hartley &
93 Chong, 2002). These extreme conditions, persistent for at least 7 Ma, longer than any other place
94 on the planet (Jordan et al., 2002; Rech et al., 2019) have exaggerated its hydrological
95 characteristics. The near total lack of vegetation and surface water other where groundwater
96 discharges, coupled with large precipitation and topographic gradients allow identification and
97 delineation of distinct groundwater systematics. Accordingly, large-scale governing mechanisms
98 are also magnified and easily characterized and constrained. The combined effect of these

99 characteristics allows fundamental properties of the system to be accurately interpreted within an
100 integrated region-wide analysis.

101 We utilize a novel and comprehensive dataset of 889 individual stable water isotope
102 samples covering approximately 28000 km². Analysis of oxygen (¹⁶O, ¹⁸O) and hydrogen (¹H, ²H)
103 isotope ratios show inflows within the basin from springs and diffuse groundwater have a
104 consistently enriched signature relative to presumed source waters revealing important
105 distinctions among inflow and recharge waters. Using the Tritium (³H) content of 87 discrete
106 water samples we show inflow waters are almost entirely ³H-dead, defining a pronounced
107 disconnect between modern inputs and groundwater in this region. These results coupled with
108 hydrophysical, geological and atmospheric data suggest that large portions of the adjacent plateau
109 are not hydraulically connected to shallow groundwaters presently discharging into SdA and
110 modern (<60 years), local meteoric inputs to the system are very limited. We present an
111 integrated conceptual model demonstrating that steady-state assumptions are inadequate,
112 watershed boundaries must be redefined and transient head-decay of groundwater storage over
113 thousand-year time scales is a critical component of the present hydrogeologic system.

114 **2. Hydrogeologic Setting**

115 Endorheic basins are topographically closed with a negative annual water balance, these
116 systems often develop salars (salt pans) at their floors (Eugster, 1980; Rosen, 1994). Local flow
117 paths mimic topography and occur between adjacent higher and lower elevation zones, while
118 regional flow paths may cross topographic boundaries (Haitjema & Mitchell-Bruker, 2005; Tóth,
119 1963). Typical of other mountainous arid regions, the SdA basin can be divided into high
120 elevation areas where most recharge occurs, a zone of lateral fluid flow and a discharge area close
121 to the basin floor (Maxey, 1968). The high vertical relief and precipitation gradients have
122 contributed to the development of a substantial regional groundwater flow system.

123 The SdA basin coincides with a sharp bend in the modern Andean volcanic arc which
124 retreats 60 km east from its regional N-S trend (Reutter et al., 2006) (Figure 1). The salar at the
125 floor of this basin covers 3000 km² at 2300 mamsl and is flanked by the Andean Cordillera
126 (~5500 mamsl) to the north, south and east and by the Cordillera de Domeyko (~3500 mamsl) to
127 the west. Its topographic watershed encompasses 17000 km², divided to the east and southeast by
128 several high volcanic peaks (Figure 1) which form the western margin of the Altiplano-Puna
129 plateau, a broad expanse of volcanic peaks and basins between 4000 mamsl and 6000 mamsl
130 (Allmendinger et al., 1997; Jordan et al., 2010). It consists of a succession of volcanic units
131 formed from large caldera forming eruptions, small volume mafic centers and numerous

132 stratovolcanoes deposited over the last 10 Ma (Strecker et al., 2007; Ward et al., 2014) and forms
133 the high peaks on the SdA topographic divide. The volcanoclastic deposits have relatively high
134 permeability (Gardeweg & Ramirez, 1987; WMC, 2007).

135 Numerous Miocene ignimbrites draped across the region and alluvial fans along the
136 flanks of SdA are important controls on springs and diffuse inflow discharging at the margin of
137 the basin floor (Jordan et al., 2002; Mather & Hartley, 2005) (Figure S1). The fractured
138 unwelded and moderately welded ignimbrites exhibit high infiltration capacity and permeability
139 providing major flow paths for local and regional groundwater, while welded ignimbrites may act
140 as local confining units (Herrera et al., 2016; Houston, 2009). Large clastic deposits, many of
141 Miocene age and buried alluvial fans such as those near the topographic divide and along the
142 margins provide substantial storage capacity and are conduits for deep groundwater transport
143 within the eastern slopes of the basin (Houston, 2009; Wilson & Guan, 2004) (Figure S1).

144 The eastern margin of the SdA basin contains several sub-watersheds delineated by a 60
145 km long N–S oriented trough in the south called the Monturaqui–Negrillar–Tilopozo (MNT); the
146 Miscanti fault and fold system to the east separates the basin from the Andes and controls the
147 development of the intra-arc lakes Miñiques and Miscanti and the broad Tumisa volcano divides
148 the northeast from the southeast sub-watersheds (Aron et al., 2008; Rissmann et al., 2015) (Figure
149 1 & S1). A large Paleozoic structural block (Peine/Cas structure), bounded by the N-S trending
150 Toloncha fault and fold system and Peine fault is interposed in the center of the southeastern
151 slope forming a major hydrogeologic obstruction that diverts, restricts and focuses groundwater
152 flow through this zone (Aron et al., 2008; Boutt et al., 2018; Breikreuz, 1995; Gonzalez et al.,
153 2009; Jordan et al., 2002; Ruetter et al., 2006) (Figure 2). The N-S fold and thrust belt
154 architecture of the basin slope forms several thrust fault systems of varying extent and depth
155 parallel to the SdA salt pan margin; these and associated lower-order faults are thought to be
156 major conduits for groundwater flow to the surface as evidenced by the spring complexes
157 emerging along or in the immediate vicinity of these zones (Jordan et al., 2002).

158 The extreme aridity of this region (on the margin of the hyper-arid Atacama Desert) is a
159 result of subsiding air within the subtropical high-pressure zone, the presence of the cold
160 Humboldt current off the Pacific coast and the Andean Cordillera acting as a high orographic
161 barrier to precipitation from the east (Garreaud et al., 2003; Hartley & Chong, 2002). Rainfall
162 varies significantly annually but on average the majority of precipitation falls during the Austral
163 summer and during La Niña episodes (Houston, 2006a; Magilligan et al., 2008). Within the
164 watershed and on the plateau, there is a strong orographic effect on precipitation. The salar
165 surface annual precipitation averages only 15 mm/year while many areas over 4500 mamsl within

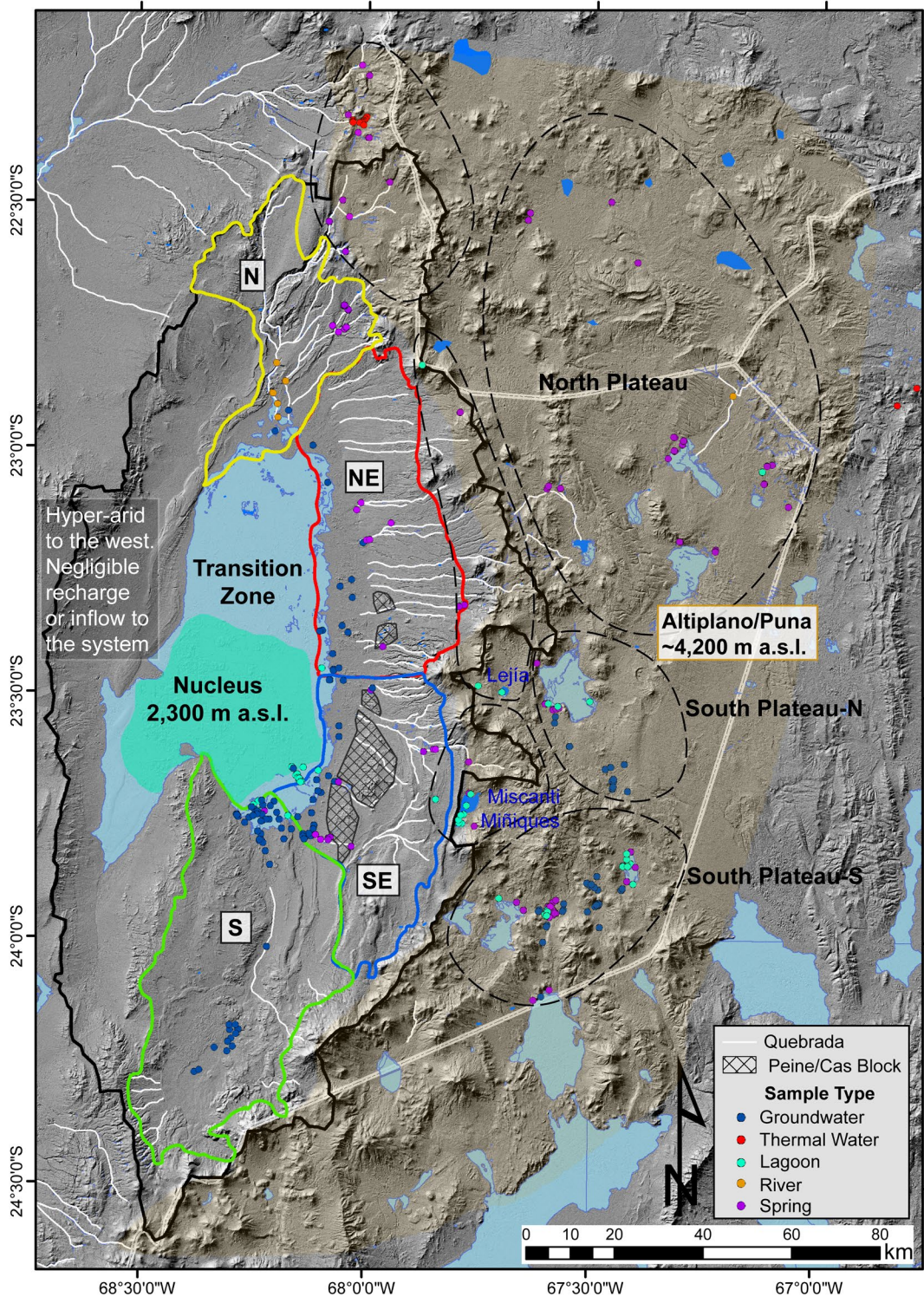


Figure 2. The SdA topographic watershed (solid black line), its recharge zones (black dashed ellipses) and discharge/inflow zones (solid colored lines). Dots represent sample sites, grouped by water type. Discharge zones extend from the salar margin to 4000 mamsl. Major drainages (quebradas and rivers) are shown in white and salars and lagoons in light blue and dark blue respectively. Notable high elevation lagoons Miñiques, Miscanti and Lejía are labeled. Surface expression of the Peine/Cas structure is hatched.

167 the topographic watershed average about 250 mm/year (DGA, 2013; Houston, 2006b). Of this
168 high-altitude precipitation approximately 50 mm to 80 mm of snow water equivalent falls each
169 year above 4500 mamsl, however much of this liquid sublimates due to high insolation and very
170 low relative humidity (DGA, 2013; Vuille & Ammann, 1997). There is no permanent ice at
171 present and it is likely that there was no glaciation in this portion of the Andes even at the highest
172 altitudes. (Ammann, et al., 2001; Ward et al., 2015).

173 Paleoclimate records indicate that hyper-arid conditions dominated prior to 325 ka in this
174 region but that a more variable climate has existed since, especially during the most recent glacial
175 cycle (Bobst et al., 2001; Lowenstein et al., 2003). During the Central Andean Pluvial Event
176 from about 18-8 ka, altiplano lake levels increased by tens of meters (Blard et al., 2011; Blodgett
177 et al., 1997; Fritz et al., 2004; Placzek et al., 2006, 2009, 2013; Sáez et al., 2016), a smaller
178 amplitude but substantial wet phase occurred around 4-5 ka (De Porras et al., 2017; Rech et al.,
179 2003). Sediment cores, rodent middens and paleo-wetland records indicate that during the
180 Holocene the climate was somewhat wetter until about 3 ka when it shifted to its modern regime
181 (Betancourt et al., 2000; Bobst et al., 2001; Latorre et al., 2003; Quade et al., 2008; Rech et al.,
182 2002). Laguna Lejía approximately 40 km east of the salar at 4325 mamsl at its late glacial high
183 stage was ~25 m higher than today which would require double the modern precipitation rate, up
184 to 500 mm/year (Grosjean et al., 1995; Grosjean & Núñez, 1994).

185 **3. Methods**

186 **3.1 Water Tracer Data**

187 Surface and groundwater samples analyzed for this study were collected during numerous
188 field campaigns between October 2011 and December 2017. In addition, we utilized all available
189 published data and reports to supplement our dataset (Table S1). Samples were collected with a
190 consistent, standardized procedure and when possible, were collected seasonally from the same
191 location. All samples were filtered through a 0.45-micron filter and groundwater samples were
192 extracted from wells screened at or below the water table with a peristaltic pump through clean
193 polyethylene tubing or with a clean bailer. In-situ measurements of temperature, specific
194 conductance, and pH were made at each sampling location during collection. Locations of all
195 stable and radioisotope water samples utilized in this work are presented in Figure 2 and detailed
196 analytical procedure for these analyses is provided in supplemental material (Text S2).

197 **3.2 Discharge Zones, Recharge Zones and Water Types**

198 Sub-watersheds (zones) of inflow to the SdA basin, designated N, NE, SE and S were
199 defined by topography, hydrogeology and isotopic characteristics (Figure 2). All shallow (<120
200 mbgl) inflow entering the basin is divided into these discrete zones corresponding closely to the
201 “watershed regions” and “groundwater flux basins” defined by Munk et al. (2018). Explicit
202 boundaries at the margins of these zones were defined by groundwater contouring and flow
203 directions determined from groundwater level measurements in the field. At high elevation, six
204 groundwater recharge zones were delineated based on topography and orientation relative to the
205 SdA watershed. Three of these zones straddle the watershed divide where hydrological conditions
206 are distinct from the plateau further east. This facilitates a detailed spatiotemporal analysis of
207 water isotope signatures among recharge and discharge waters, allows for an examination of
208 sources and flow paths and ultimately to constrain dominant hydrological mechanisms within and
209 between these zones.

210 All data were categorized into six water type groupings (Groundwater, Spring, Spring-fed
211 River, River, Lagoon and Thermal) designed to facilitate inter-comparison and interpretation of
212 results. Almost no vegetation exists except where fresh water bodies intersect the surface,
213 consequently, these water classifications were reliably determined with the use of satellite
214 imagery and field observations. Groundwater is herein defined as samples taken directly from
215 wells (e.g. monitoring, pumping) that are open to the aquifer at depths ranging from 1 to ~120
216 mbgl. Spring water denotes perennially flowing groundwater discharge and Spring-fed Rivers are
217 waters fed predominantly by groundwater discharge a short distance upgradient (<1 km) of where
218 it was sampled. These waters are herein grouped with Spring waters because our analysis shows
219 them to be isotopically indistinguishable. Rivers are defined as large systems of perennially
220 flowing surface waters on the order of 10 to 50 km in length. Lagoons are surface water which is
221 perennially extant at the surface, including freshwater lakes, wetlands and brackish-to-salt
222 lagoons. Thermal waters are from geysers or thermal pools directly influenced by geothermal heat
223 with temperatures between ~40° to ~80° C. The distinction between these water types is based on
224 extensive knowledge of the regional hydrogeology gathered during more than ten field
225 campaigns, previous published work and scrutiny of isotopic signatures.

226 3.3 Atmospheric Back-Trajectory Modelling

227 To constrain prevailing atmospheric moisture sources in the modern climate system we
228 calculated 5-day air parcel back-trajectories using NOAA Air Resources Laboratory’s HYSPLIT
229 Transport and Dispersion Model for all large and extensive precipitation events in the region over

230 the past 20 years (1997-2017) (DGA, 2013; Draxler & Hess, 1998). More detail is provided in
 231 supplementary material (Text S2).

232 4. Results

233 4.1 Tritium

234 We collected an exhaustive set of water samples from the SdA watershed and analyzed
 235 them for the ^3H isotope content of the water molecules, using these ^3H values as a direct tracer of
 236 Mean Residence Time (MRT) and source (Table 1). We determine a “percent modern water”
 237 (R_{mod}) in these samples not as a direct estimate of ratios of modern water content but rather as a
 238 relative value to compare connections with modern meteoric inputs. To determine R_{mod} we first
 239 constrain the average ^3H content of modern precipitation in this region. This value, also presented
 240 by Boutt et al. (2016) was determined to be 3.2 ± 0.6 TU (1σ) from five carefully chosen rain
 241 samples collected during 2013 and 2014 (locations in Figure 3). This agrees with the range of
 242 values from Cortecci et al. (2005), Grosjean et al. (1995), Herrera et al. (2016) and Houston
 243 (2002, 2007). We use a value on the lower end of the published range (3.23TU) based on the
 244 assumption that smaller precipitation events are unlikely to produce actual recharge in this
 245 environment and events with the lowest TU values (sourced from the Pacific Ocean) are
 246 reflective of decade-scale bias from ENSO conditions not the average (Houston, 2007). We
 247 assume this meteoric input value is roughly representative of average precipitation from about
 248 1990 to present because the bomb peak signature is no longer resolvable after that date in the
 249 southern hemisphere, and also representative of average precipitation before the mid-1950’s since
 250 the bomb peak had not yet occurred (Houston, 2007; Jasechko, 2016). Water recharged in 1955
 251 prior to the bomb peak with a ^3H content of 3.23 ± 0.6 TU would have between 0.8 and 0.11 TU
 252 in July 2018 (Stewart et al., 2017).

Data Included with Manuscript Submission

Table 1. ^3H data from waters collected in this study and from Grosjean et al., 1995. Column ^3H contains analytical results, *Error* the analytical error associated with each analysis, $^3\text{H}^*$ is the ^3H value decayed to a common date and $R_{\text{mod}}\#$ is the relative ratio of modern water in each sample.

253 This pre and post-bomb *background* ^3H production temporally constrains the meteoric
 254 input value, but there is also a potential source of ^3H that is produced within the aquifer from ^6Li
 255 neutron flux; this *in-situ* production from water-rock interaction is generally assumed to be very
 256 small but given the Li-rich aquifer material in this region we consider it a potential factor in the
 257 maximum apparent *background* ^3H threshold (Boutt et al., 2016; Houston, 2007). By assessing
 258 the ^3H content of SdA nucleus brine samples which have been determined to be $\gg 60$ years old

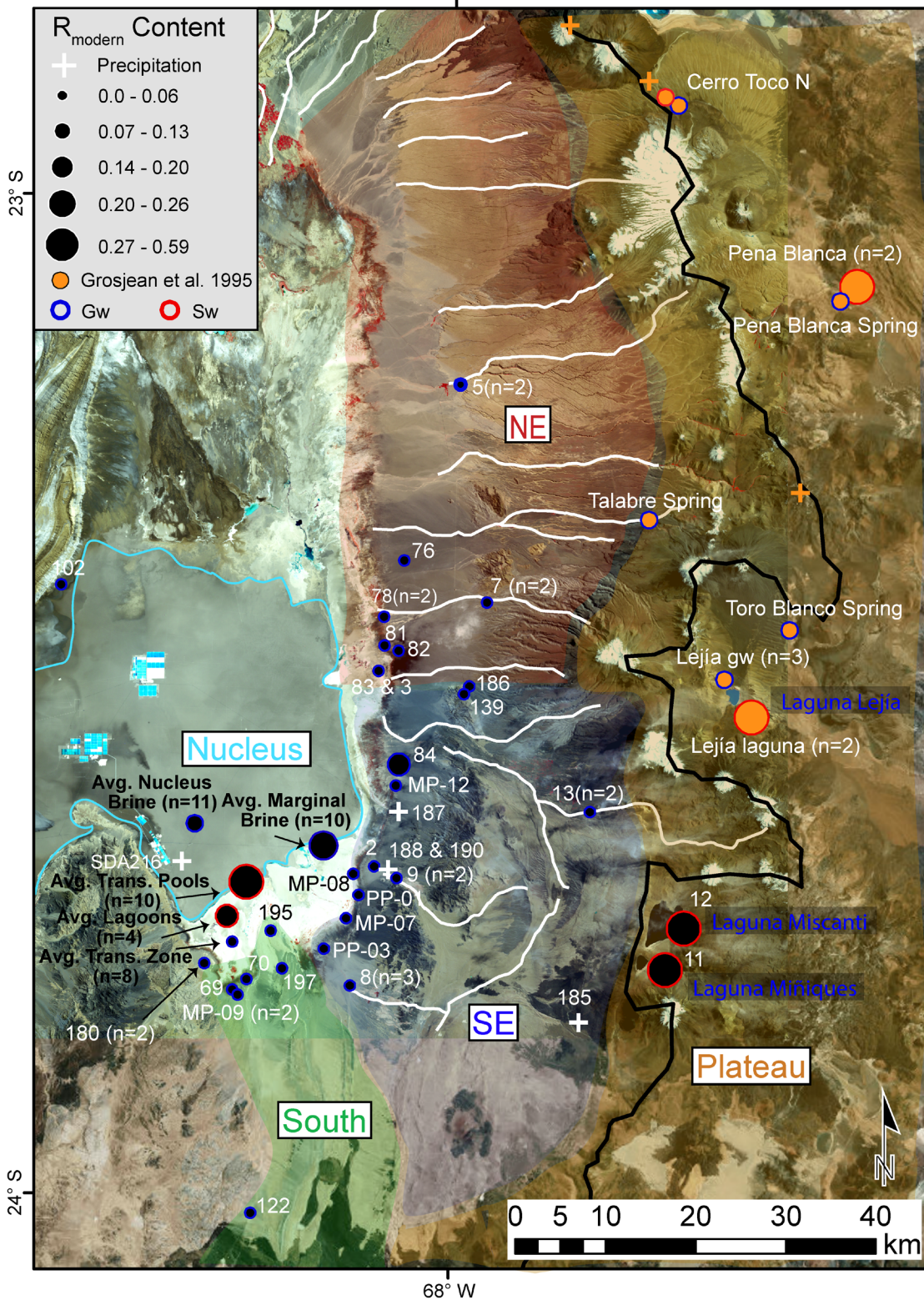


Figure 3. Modern water content in samples (n=87) proportional to circle size. Shaded areas are inflow water zones. Data from Grosjean et al. (1995) are orange. Circles in Nucleus and Transition Zone represent average of water groupings. Surface waters (sw) are outlined in red, groundwaters (gw) in blue.

260 through other methods, we can establish the cutoff for this *in situ* production to be approximately
 261 0.15 TU (Boutt et al., 2016; Houston, 2007; Munk et al., 2018). Therefore, values less than 0.15
 262 TU are essentially indistinguishable from 0.0 TU due to this potential *in situ* production in waters
 263 containing effectively zero water volume recharged post-1955; waters below this threshold are
 264 interpreted to be ³H–dead. Nearly all waters sampled in this analysis contain very low levels of
 265 ³H and therefore very small fractions of modern water if any at all; because of this our objective
 266 is not to directly estimate discrete MRT distributions or the “percent modern” component of these
 267 waters (Cartwright et al., 2017). Instead we quantify the relative amount of modern water present
 268 to constrain connections to modern meteoric inputs among the surface and groundwater bodies
 269 and connections between these systems.

270 All ³H samples are allocated to nine distinct water “bodies” representing the major water
 271 compartments in the basin. These groundwater and surface water bodies, corresponding closely
 272 to those discussed by Boutt et al. (2016) and Munk et al. (2018) are hydrogeologically distinct,
 273 formed and sustained by a unique set of hydrological processes. Waters are grouped into (Figure
 274 3): Nucleus Brines, a very dense brine (>200 mS/cm SC) within the core of the evaporite aquifer;
 275 Marginal Brines, a dense brine in the transition between the Nucleus Brines and fresher
 276 Transition Zone waters; the Transitional Pools, highly saline (>200 mS/cm SC) surface waters at
 277 the margin of the nucleus surficial halite deposit, in the southeast zone of the salar these waters
 278 occupy about 0.2 km² of surface area. Landward of these Transitional Pools are several large
 279 brackish-to-salt Lagoons, shallow surface water bodies which occupy about 0.5 km² and host
 280 important wildlife such as flamingos and brine shrimp. Transition Zone waters are shallow
 281 brackish groundwaters within the surficial gypsum dominated zone between the nucleus and the
 282 edge of the basin floor; South Inflow and East Inflow are fresh groundwater-fed discharge waters
 283 entering the basin below ~3000 mamsI; High Elevation Inflow waters are fresh groundwater-fed
 284 discharge higher on the eastern slope of the basin; and the High Elevation Lakes are fresh-to-
 285 brackish lake waters just outside the watershed divide.

286 All ³H data for each of these water bodies is summarized in Tukey Box Plots and plotted
 287 along a transect through the eastern margin (Figure 4). Results show that waters discharging
 288 along the eastern margin have values indistinguishable from zero as nearly all fall fully below the
 289 background threshold described above. The only two samples (73 & 84) which have substantially
 290 higher values and the few that are borderline above the background, in the Transition Zone and
 291 the East Inflow are in the proximity of preferential flow paths related to rapid infiltration of
 292 modern precipitation into permeable alluvial fans, a process indicated by Boutt et al. (2016). The

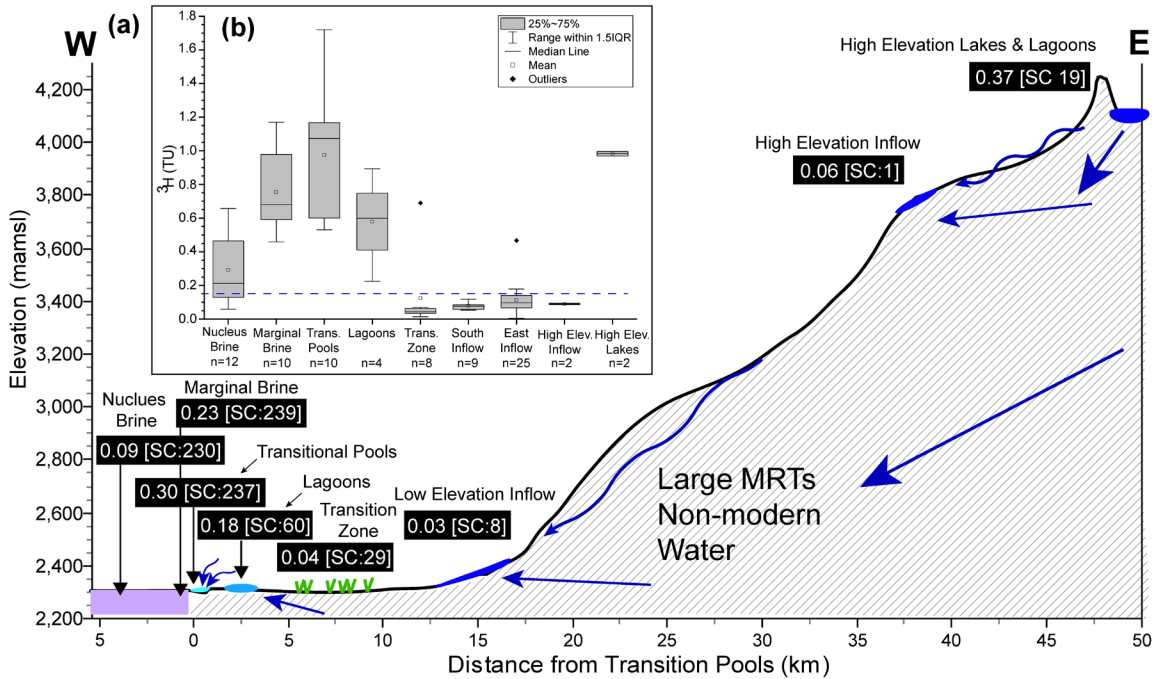


Figure 4. (a) Modern water proportion (R_{mod}) among groundwater and surface water bodies along transect of eastern SdA margin. South Inflow and East Inflow waters are averaged as a single low elevation inflow water body. Mean R_{mod} value of each water grouping (in black rectangles) and mean Specific Conductivity (SC) in mS/cm. **(b)** Tukey box plot of 3H content (TU) in these water bodies. Blue dashed line is the theoretical maximum limit (0.15TU) of background 3H produced in-situ water-rock interaction.

293 data from high elevation lakes Miñiques and Miscanti (samples 11 & 12) as well as other surface
 294 waters at high elevation (Laguna Lejía & Pena Blanca) show much higher values, similar to the
 295 average of the Transitional Pools waters. Nucleus Brine waters are predominantly composed of
 296 pre-modern groundwater with a small component of modern water in some samples, the
 297 Transition Zone waters are entirely pre-modern while the Lagoons have a large component of
 298 pre-modern water but contain a somewhat larger amount of modern water.

299 The spatial coverage and density of samples across the eastern margin, considering the
 300 focused nature of groundwater discharge in SdA gives confidence that shallow inflow to the salar
 301 is well-represented by this analysis and that nearly all of it is composed of pre-modern. It
 302 is also apparent that surface waters (Laguna Miñiques, Miscanti, Lejía and the Transitional Pools)
 303 have an analogous signature of about 0.30-0.40 R_{mod} . The consistent signature in these waters
 304 highlights and defines the substantial contrast between the surface water system and groundwater
 305 system (surface water sample “Cerro Toco N” is the exception to this, likely primarily composed
 306 of water sourced from the “Cerro Toco N” groundwater just upgradient) (Figure 3). The
 307 interaction of these surface and groundwater systems serve to illuminate hydrological

308 mechanisms governing the system as a whole and constrain the distribution of modern water
 309 within its sub-systems.

Elevation of Lakes (mamsl):		Hydraulic Conductivity [K]:				
	4150	K= 15.5 m/d		K=5.0 m/d	K=1.0 m/d	K=.01 m/d
Sample Site (name)	Elevation (mamsl)	Distance from Lakes (km)	v (m/d)	v (m/d)	v (m/d)	v (m/d)
13 (Socaire)	3606	12	5.0	1.6	0.32	0.0032
9 (Peine)	2450	29	6.5	2.1	0.42	0.0042
8 (Tilomonte)	2373	33	6.0	1.9	0.38	0.0038
84 (Truck)	2329	34	5.9	1.9	0.38	0.0038
Sample Site (name)	Hydraulic Gradient [dh/dl]		MRT (yrs)	MRT (yrs)	MRT (yrs)	MRT (yrs)
13 (Socaire)	0.045		7	20	101	10146
9 (Peine)	0.059		12	38	190	18962
8 (Tilomonte)	0.054		15	47	235	23490
84 (Truck)	0.054		16	49	243	24333
Sample Site (name)	Distance from Lakes (km)	³ H* (TU)	MRT w/ Lake Water Input (yrs)	MRT w/ Precipitation Input (yrs)	v (m/d)	
					Assuming ³ H-Calculated MRT (w/ lake water)	Assuming ³ H-Calculated MRT (w/ precip.)
Precipitation [N _o]	0	3.23	-	-	-	-
11 & 12 (Miñ./Mis.) [N _o]	0	0.67	-	-	-	-
13 (Socaire)	12	0.07	40	68	0.8	0.5
9 (Peine)	29	0.04	48	76	1.7	1.0
8 (Tilomonte)	33	0.08	37	65	2.5	1.4
84 (Truck)	34	0.32	13	41	7.2	2.3

Table 2. Calculations of transit time estimates assuming piston flow and a decay constant. High elevation lake water ³H value and modern meteoric water are used as input water ³H values. These input ³H values were decayed and seepage velocities (v) estimated with aquifer properties (K & θ) from Houston (2007) and a plausible range of values. Velocities calculated by piston flow transit times, then MRT of waters estimated under these conditions.

310 Since the groundwater can only be directly measured at discrete points and processes in
 311 the thick vadose zone are not easily constrained, simple analytical representations with a range of
 312 plausible hydrologic properties can facilitate interpretation of dominant processes controlling
 313 flow paths, MRTs and sources of groundwater inflow. Along a cross-section from the
 314 Transitional Pools to the High Elevation Lakes (Figure 4) we estimate the MRT of sampled
 315 groundwater discharge assuming a shallow flow path (<100 m), piston flow and a plausible range
 316 of hydraulic properties (Table 2). The MRT estimates for each groundwater discharge site were
 317 calculated independently using the observed ³H values, estimated seepage velocities and
 318 measured hydraulic gradients (Table 2).

319 If we first assume the ³H value of recharge water lies somewhere between modern
 320 precipitation and high elevation surface waters (as focused recharge from these waters bodies is
 321 thought to be very important), it will decay according to this formula as it moves downgradient;
 322 where t = time, N = sample ³H value, N_o = initial ³H value and λ = the decay constant of ³H:

323
$$t = \frac{\text{Ln}(N/N_o)}{-\lambda}$$

324 We then estimate how long it would take for that water to decay enough to match the ^3H value
325 measured in groundwater discharging downgradient. This MRT is not intended to physically
326 replicate the complexity of groundwater transport but paired with a range of seepage velocities,
327 places critical constraints on plausible MRTs. Using estimated effective porosity (θ) and a range
328 of hydraulic conductivities (K) including values previously determined by Houston (2007) in a
329 basin just north of SdA, we calculated a seepage velocity for each sample site:

330
$$v = (K/\theta) \times (\delta h/\delta l)$$

331 We then determined what seepage velocity would be required for each flow path to reflect the
332 MRT at each site estimated by simple ^3H decay. Lastly, we calculated the MRT for each sample
333 using these estimated seepage velocities.

334 These results indicate that simple piston flow and ^3H decay predict a sizeable portion of
335 young water not observed at these sites and would require seepage velocities much greater than
336 would be reasonable in this environment. Two factors would suggest that actual MRTs of these
337 waters resemble something closer to those predicted with the lowest velocities in Table 2. ^3H
338 values in inflow waters are well below the background production envelope but are rarely always
339 zero, therefore the value used for those sites may be artificially high as some or all of the ^3H in
340 these waters is potentially derived from *in situ* production or analytical uncertainty while its
341 modern water content may in fact be approaching zero. The thick vadose zones in this
342 environment may require hundreds of years or more for water to infiltrate (Herrera et al., 2016;
343 Walvoord et al., 2002) leading to effective seepage velocities much smaller than reasonable K
344 values in Table 2 would predict. Together this suggests that our ^3H observations at these
345 groundwater discharge sites cannot be explained by modern high elevation recharge flowing
346 downgradient and becoming low elevation discharge within modern time frames; under the most
347 plausible hydrogeologic conditions, it likely requires hundreds to thousands of years for high
348 elevation recharge to reemerge in the SdA watershed as springs and diffuse groundwater.

349 4.2 Stable Isotopes of Water

350 In this groundwater dominated system, isotopic signatures of individual samples are
351 primarily a reflection of its source water mixture and flow path characteristics. Comparing
352 signatures in each discharge zone (N, NE, SE and S) and recharge zone (North Divide, NE
353 Divide, SE Divide, North Plateau, South Plateau-N and South Plateau-S) we can address
354 important questions regarding dominant hydrological mechanisms governing the larger orogenic-
355 scale groundwater system. It is important to note that the western half of the basin is not included

356 in our analysis of the SdA system because the actual inflow to the basin from that region is
 357 negligible when compared to the other zones, accounting for less than 1% of the total (Munk et
 358 al., 2018) (Figure 2).

359 $\delta^2\text{H}$ data from the major groundwater discharge sites (springs) in the NE and SE zones
 360 measured seasonally over a nearly 7-year period and more sporadically back to 1969 show
 361 consistent values with some correlation to large local precipitation events but the responses are
 362 short-term (Figure S2). The documented major precipitation events in March 2012 and March
 363 2015 appear to show excursions of $\sim 5\text{‰}$ in $\delta^2\text{H}$, after which data revert to the long-term trend in
 364 less than a year. This suggests the signature of local meteoric infiltration is observed at these sites
 365 below 3000 mamsl but is largely restricted to short time-scales and that longer flow path waters
 366 are the principal control on isotopic values of inflow water. Data from the sample sites within the
 367 NE and SE zones have a mean standard deviation of 2.2‰ and 2.8‰ in $\delta^2\text{H}$ respectively,
 368 reflecting variability between sites and the short-term influence of local recharge pulses. Stream
 369 gauge data at the Spring-fed streams also show influence from local recharge events but revert to
 370 a consistent long-term average value quite rapidly (DGA, 2013). Since this analysis utilizes a
 371 large dataset collected consistently over more than 20 years, we are confident that our analysis of
 372 environmental tracers reflects the long-term average discharge signal of the groundwater system.

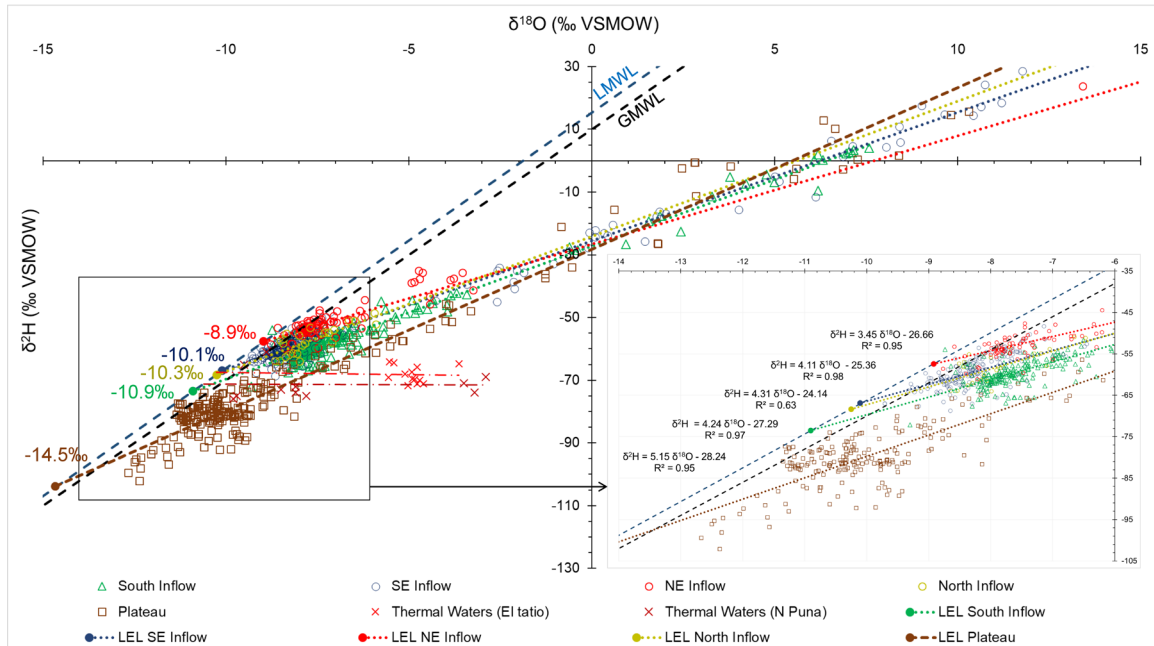


Figure 5. All water stable isotope data from the SdA regional watershed (n=889). Colors correspond to the three inflow zones labeled in Figure 2, brown points are all plateau waters. Meteoric source water isotopic signature is estimated for each zone where LEL intersects the Local Meteoric Water line (LMWL) of Chaffaut et al. (1998). High temperature waters from the EI Tatio thermal field and northern Puna region indicated by red Xs.

373 All $\delta^2\text{H}$ and $\delta^{18}\text{O}$ data analyzed in this work are presented in Table S2, and are plotted in
374 $\delta^2\text{H} - \delta^{18}\text{O}$ space along the GMWL and the modern Local Meteoric Water Line (LMWL) in
375 Figure 5 (Chaffaut et al., 1998). To a first order it is apparent that a linear fit of all these data
376 forms a line which is slightly offset below but parallel to the LMWL; this phenomenon has been
377 observed by several other workers in this basin and in other arid basins in the central Andes and
378 worldwide (Aravena, 1995, 1999; Boschetti et al., 2007; Fritz et al., 1981; Koeniger et al., 2016;
379 Margaritz et al., 1989). Also evident in these data is a bimodal distribution; one cluster is
380 isotopically more depleted, centered around -80‰ $\delta^2\text{H}$ and the other around -60‰ $\delta^2\text{H}$.
381 Distinctions can also be identified between zones of inflow which indicate important spatial
382 differences in discharge within the SdA watershed.

383 The strong influence of kinetic fractionation due to evaporation in this region allows for
384 back calculation of the expected meteoric source waters for each of these zones (Text S4). By
385 defining a regression by the waters of each zone we can predict the meteoric source $\delta^{18}\text{O}$ and $\delta^2\text{H}$
386 signature while also determining the slope characteristic of evaporative fractionation in each.
387 Coefficients of determination (R^2) show our regressions describe the data well (0.95-0.98), except
388 in the North zone (0.63) for which there is less confidence due to a relative lack of data ($n=24$).
389 The four inflow water zones are defined by slopes of: 3.5 (NE), 4.1 (SE), 4.2 (S) and 4.3 (N)
390 while plateau waters show a steeper slope of 5.2 (Figure 5). These values are consistent with
391 empirically derived Local Evaporation Lines (LEL) from this region and similar environments
392 (Aravena, 1995, 1999; Boschetti et al., 2007, 2019; Ortiz et al., 2014; Scheihing et al., 2017).
393 Shallower slopes reflect the higher average annual temperatures and lower relative humidity of
394 the lower elevations, the much steeper slope of high-altitude plateau waters reflects the higher
395 average relative humidity and lower temperatures there, and associated smaller kinetic effects.
396 Predicted source waters derived by projecting these regressions to their intercepts with the
397 LMWL show that the meteoric source of the plateau water is substantially more depleted than
398 those of discharge waters within the SdA basin. Inflow waters are more enriched by about 5.6‰
399 (NE), 4.4‰ (SE), 4.2‰ (N) and 3.6‰ (S) in $\delta^{18}\text{O}$ than average plateau waters. We can therefore
400 deduce that substantial hydrogeological distinctions exist between these two systems.

401 To refine the distinctions among recharge waters and to relate these characteristics
402 spatially we compare signatures of the three recharge zones on the plateau and the three in the
403 region straddling the divide. Again, plotted in $\delta^2\text{H} - \delta^{18}\text{O}$ space we compute the predicted
404 meteoric source of each recharge zone (Figure 6). These results show that waters of the divide
405 predict source waters comparable to the waters discharging directly downgradient in the basin,

406 implying that the predominant source signature of these waters is largely analogous. In
 407 comparison, the three zones on the plateau show a substantially more depleted signature
 408 suggesting these waters have a different meteoric source from both the inflow waters and the
 409 divide waters. The zone covering the largest area of any (North Plateau) appears to have the least
 410 isotopic similarity to the SdA watershed inflow with values between 5.2‰ and 7.2‰ more
 411 depleted in $\delta^{18}\text{O}$. Further statistical scrutiny of these data provides better definition of these
 412 distinctions.

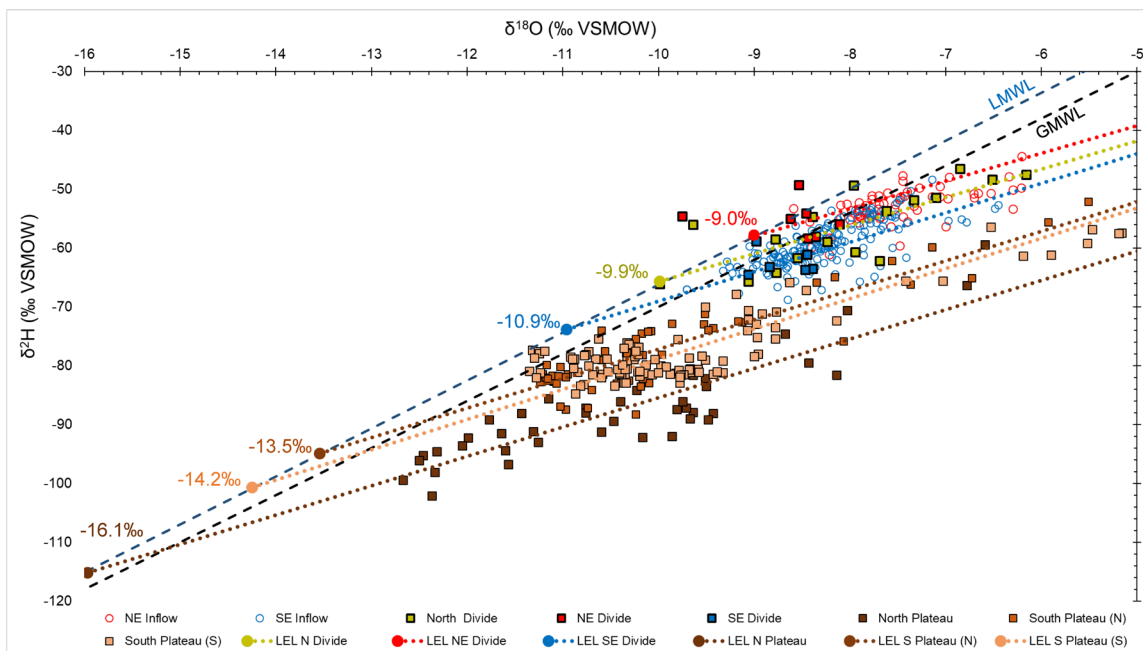


Figure 6. All stable water isotope data from plateau and divide recharge zones. Inflow waters (NE and SE zones) are red and blue points displayed for context with inflow. Predicted meteoric source waters from LEL intercept with LMWL are colored numbers.

413 $\delta^{18}\text{O}$ data from all zones were filtered with the deuterium-excess (d-excess) parameter
 414 and summarized statistically (Figure S3). Separating samples with a d-excess less than zero is
 415 considered the optimal point for removing most kinetic influences while maintaining the
 416 maximum number of samples uninfluenced by evaporative effects (Jasechko et al., 2014).
 417 Removing the kinetic evaporative influence from our dataset allows for direct comparison
 418 between inflow waters by including only those most representative of their original meteoric
 419 source. This analysis provides further evidence of the large statistical distinctions between all
 420 SdA inflow water and waters on the plateau, also that there is less apparent distinction between
 421 the inflow and the divide waters. We find the mean $\delta^{18}\text{O}$ value of NE inflow zone water is about
 422 1.3‰ more enriched than the divide waters upgradient of it, the SE inflow waters are about 0.4‰
 423 more enriched than its corresponding divide waters and the N zone waters appear very similar to
 424 its corresponding divide zone waters. There is also a clear statistical distinction between the NE

425 and SE inflow waters, one which is also exhibited by the calculated meteoric source showing the
 426 mean of the NE waters is more enriched than the mean SE waters by about 1‰. This suggests
 427 meaningful differences between sources and/or groundwater mechanisms governing the NE and
 428 SE inflow waters.

429 These same d-excess filtered data from each compartment were compared using an
 430 unequal variances t-test (Welch’s test) to assess the null hypotheses that samples within each zone
 431 represent waters from the same population. $\delta^2\text{H}$ and $\delta^{18}\text{O}$ values of these water groupings were
 432 compared: All Divide - All inflow (N, NE, SE, S); All Plateau – All Inflow; All Divide – All
 433 Plateau; NE – SE and SE – S. Results show strong statistical difference ($P < 0.0001$) between all
 434 these zones except for All Divide – All inflow ($P=0.035$) for both $\delta^2\text{H}$ and $\delta^{18}\text{O}$ and SE – S
 435 ($P=0.164$) for $\delta^2\text{H}$ values only. Divide waters and inflow waters are not statistically different in
 436 terms of $\delta^2\text{H}$ or $\delta^{18}\text{O}$, S and SE waters are distinct with respect to $\delta^{18}\text{O}$ but not distinct with
 437 respect to $\delta^2\text{H}$, which indicates a distinct hydrological process may be further influencing waters
 438 in the South zone.

439 To compare groundwater flow paths into the basin, we trace the isotopic evolution of
 440 waters moving through each inflow zone. Figure 7 shows $\delta^{18}\text{O}$ by sample elevation for each
 441 inflow zone and the recharge waters upgradient of them. Waters in each zone show a general
 442 trend of increasing salinity with decreasing elevation toward the SdA basin aquifer. This trend is

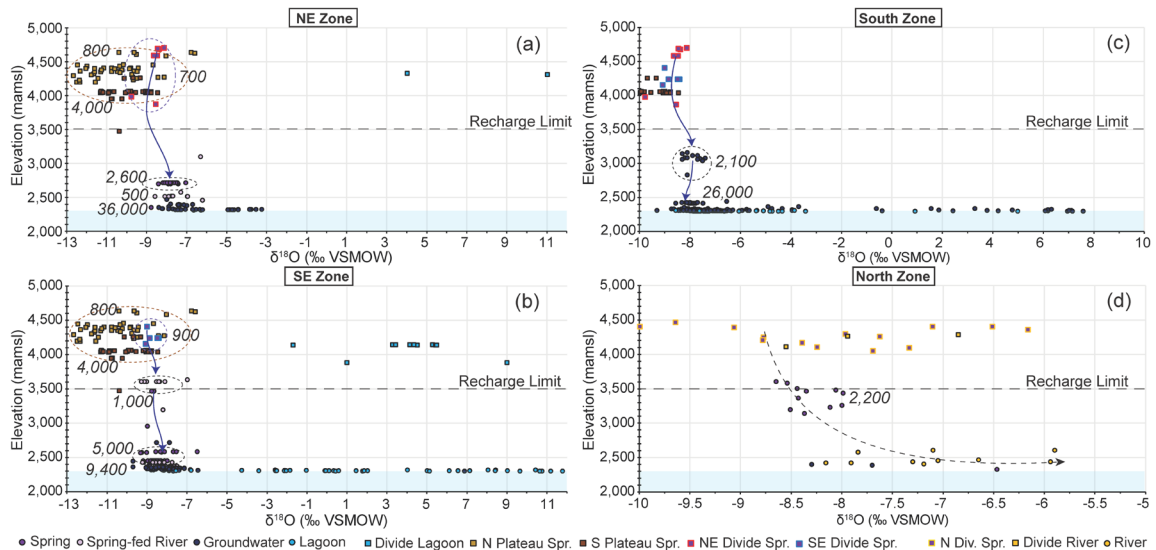


Figure 7. $\delta^{18}\text{O}$ in waters from each zone plotted against sample elevation. Recharge limit line denotes elevation below which no significant recharge occurs. Blue shaded envelope represents the salar evaporite aquifer below the basin floor. Specific Conductivity ($\mu\text{S}/\text{cm}$) of sample groupings in italics. Ellipses in (a), (b) and (c) indicate descriptive groupings discussed in text and blue arrows indicate general hydrochemical evolutionary pathways. Dashed slope in (d) indicates predicted trend of isotopic evolution. Water types and locations are labeled in legend (Spr.=Spring water).

443 expected as more dissolved solids can be accumulated in groundwater as it incorporates ions from
444 rock weathering and re-mobilizes residual salts present in the aquifer material. While a
445 substantial increase in salinity downgradient indicates waters are evolving geochemically, very
446 little isotopic evolution is observed between recharge and discharge waters. This has been
447 observed in previous work in this region, suggesting increasing salinity with no isotopic evolution
448 reflects “salinization” of fresh groundwater inflows not evaporative enrichment (Fritz et al., 1978;
449 Risacher et al., 2003). The evolution observed in the NE, SE and S waters show that
450 groundwaters discharging near the salar margin have a direct relationship to that of groundwaters
451 in the divide recharge area upgradient but not the majority of the plateau waters. The overlap that
452 occurs between some plateau waters and divide waters, especially in the SE suggests there is at
453 least some connection between portions of the plateau and the SdA inflow. The south zone
454 displays similar characteristics to the NE and SE but also a slight de-evolution of waters from the
455 groundwater in the central MNT aquifer to discharge near the Tilopozo wetland. In the N zone
456 where two large perennial rivers flow to the basin floor, waters follow a trend more typical of a
457 surface watershed where the lower reaches are more steadily isotopically evolved due to strong
458 evaporative enrichment. $^{87}\text{Sr}/^{86}\text{Sr}$ data presented by Munk et al. (2018) indicate that some of the
459 sub-basins (e.g. Miscanti) on the divide and plateau have direct geochemical connections to
460 downgradient inflow areas, while others appear quite disconnected. Since very little actual
461 recharge occurs where annual precipitation is less than 120 mm/year (equating to an elevation of
462 ~3500 mamsl), these results suggest the predominant source of inflow is upgradient groundwaters
463 not local inputs (Houston, 2007; Houston & Hart 2004).

464 4.3 Constraining Modern Meteoric Inputs

465 Air mass tracking of major precipitation events reveal macro-scale features of the modern
466 climate regime and allow for comparison between meteoric recharge inputs to the plateau and
467 ultimately the inflow zones (Figure S4). Our results indicate that nearly all precipitation is
468 derived from either the northeast or east and any distinctions in meteoric input signatures to this
469 system are more the consequence of localized convective and orographic effects, not
470 distinctions between initial moisture source. Prominent orographic barriers exist along the length
471 of the watershed divide and along a NW to SE trending chain of volcanoes to the east of Laguna
472 Miñiques which may develop distinctive average meteoric input signatures among recharge zones
473 and inflow waters to the SdA basin.

474 5. Discussion

475 Our integrated analysis of stable and radiogenic water isotope systematics in the SdA
476 regional watershed defines the spatiotemporal dimensions of dominant sources and flow paths,
477 the distribution and degree of connection among water bodies, sub-catchments and perched
478 basins on the Altiplano-Puna plateau, and distinctions between the modern and paleo-
479 hydrological systems. We show that inflow to the basin is not predominantly composed of
480 recharge on the plateau, modern recharge (<60 years old) on the high elevation watershed divide
481 or local, modern inputs within the watershed. Therefore, the draining of groundwater storage
482 must be a critical component of the present water budget. We also propose that influx of solute-
483 rich underflow from high elevation basins, predominantly in the southern and eastern regions
484 over long time-scales is an important mechanism to account for the large solute (Na and Cl)
485 imbalances observed in hydrological budgets (Munk et al., 2018). These governing mechanisms
486 are defined in a fully integrated conceptual model of the hydrologic system as it currently exists,
487 placing critical constraints on fundamental hydrological processes controlling orogenic-scale
488 groundwater systems (Figure 8). Our results reveal novel insights about these large-scale systems
489 and provide a framework within which to address important unresolved questions in these basins
490 worldwide.

491 Analysis of ^3H in water, the long-term stability of isotopic signatures in groundwater
492 discharge and the almost total lack of direct recharge occurring at low elevations indicate that
493 inflows from the southern and eastern margin of SdA are principally composed of pre-modern
494 recharge (>60 years old). These inflow waters which represent a large portion of total water
495 (~65%) and solute flux into the basin are, principally, expressions of a regional hydrologic system
496 decoupled from modern inputs (Munk et al., 2018). Surface waters bodies at high and low
497 elevations (Laguna Miñiques, Miscanti, Lejía and the Transitional Pools) appear to have a
498 consistent signature of about 30% modern, reflecting a dynamic equilibrium between ^3H -rich
499 modern recharge, ^3H -dead groundwater inflows and discharge fluxes. This fairly uniform
500 signature among waters which have direct connections to modern meteoric inputs, highlights a
501 clear contrast between surface water systems and the larger groundwater system. The prevalence
502 of pre-modern water observed in inflow to the basin, the timing of past pluvial periods (>1000
503 yrs.), very thick vadose zones (up to 1000 m or more) and the large scales over which these flow
504 paths must develop reveal a groundwater system which operates over time scales on the order of
505 100-10,000 years or longer. Taken together, these results indicate that the SdA hydrologic
506 system is heavily groundwater dominated and compartmentalized by source and flow path over
507 small spatial and vertical distances.

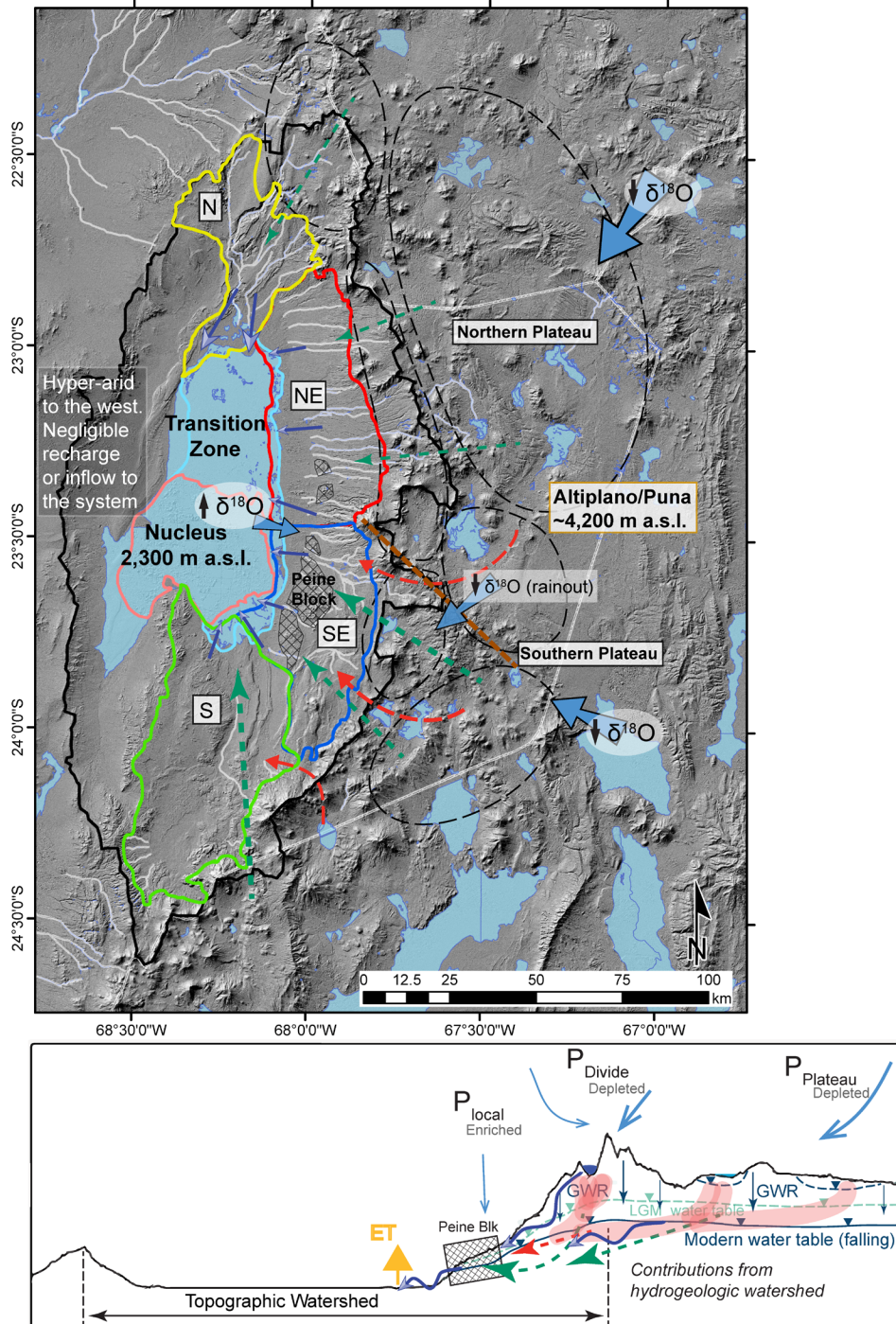


Figure 8. Conceptual model of integrated SdA regional groundwater system. Major mechanisms governing the contemporary hydrologic system and their relative influence. Shown in plan view (a), solid light blue arrows represent the distribution of modern meteoric inputs and their signatures, brown dashed line denotes a major orographic barrier to precipitation east of Miñiques and Miscanti lakes. Solid blue arrows represent inflows of modern recharge, green dashed arrows are major inputs of paleo-groundwater, red dashed arrows show hypothesized influx of solute-rich fluid. (b) Cross-sectional view of the SE zone shows the distribution and relative importance of these hydrological mechanisms. Blue lines are the estimated position of the modern water table, green is the LGM water table and the corresponding flow paths of modern and paleo-groundwater, red is solute-rich influx.

509 Large infrequent precipitation events observed and described by Boutt et al. (2016) and
510 others which do infiltrate and move along preferential flow paths near the margin of the evaporite
511 deposit are focused in nature and governed by the presence of alluvial fans with high infiltration
512 capacities and by sharp saltwater-freshwater interfaces created by the dense brine of the evaporite
513 aquifer. These interfaces which exist near the surface in the transition zone are quite stationary
514 and restrict infiltration of fresher water, creating pathways of preferential flow on the margins of
515 the salar (McKnight, 2019). These modern meteoric inputs are directly reflected in the elevated
516 ^3H values observed in the Transitional Pools near the margin of the salar nucleus, the slightly
517 elevated ^3H values in some lagoon waters and in isolated shallow groundwater in some alluvial
518 fans. The lagoons respond to this focused infiltration and flow by occasionally flooding during
519 extreme precipitation events near the basin floor but return to their original shape and volume
520 quite quickly. This is supported by the findings of Boutt et al. (2016) showing responses in the
521 shallow brine aquifers to large precipitation events on the salar are muted and short-lived and that
522 the groundwater dominated lagoons show little permanent response to these events. Lagoon water
523 ^3H compositions show they are predominantly composed of pre-modern groundwater inflow and
524 that flood water likely exists as a focused lens above the much denser lagoon water directed by
525 the low permeability gypsum covering much of the transition zone surface. The few Transitional
526 Pool waters which were sampled just below the land surface south of the open pools appear to
527 contain substantial amounts of this pre-modern water as well the lagoon sample “La. Brava B”
528 which was taken from a shallow arm of the lagoon in the path of one of these focused meteoric
529 water flowpaths. The waters along the transition zone-nucleus margin are controlled by
530 exchanges between these modern meteoric water lenses and pre-modern groundwater inflow from
531 below. The ^3H content of lagoon waters and waters in the transition zone subsurface likely reflect
532 mixing of small volumes of these modern meteoric water lenses with a much larger volume of
533 pre-modern inflow. Though the specific dynamics of these lenses and their interaction with
534 groundwater requires further inquiry, there is ample evidence that modern water effectively
535 bypasses the lagoons themselves in these shallow modern water lenses and migrates toward the
536 Transitional Pools where it dissolves and infiltrates through the porous halite units at the nucleus
537 margin.

538 Recent research of global climate change indicates that this region of the Andes and
539 Preandean depression is predicted to see an increase in overall moisture and also large
540 precipitation events due to the southward shift in the South American Monsoon (Jordan et al.,
541 2019; Langenbrunner et al., 2019; Pascale et al., 2019). The substantial increase in extreme
542 precipitation events observed since 2012, with one 4-day event in February 2019 recording

543 ~100mm of rain on the salar surface which normally receives only 15 mm/year (personal
544 communication with Albemarle corp., July 2019), may in fact be a direct result of these large-
545 scale climate changes and are likely to continue. The recent observations of persistent surface
546 water expansion in the transition zones of SdA may also be a result of these decadal-scale
547 changes in meteoric inputs, not a direct result of extractions from the brine aquifer or long-term
548 changes associated with fluctuations in paleo-groundwater inflow.

549 Region-wide analysis of stable isotope systematics reveal that each water inflow zone is
550 defined by a distinct combination of sources and flow paths relating directly to their geology,
551 meteoric inputs and connections to high elevation sub-basins beyond the watershed divide. Our
552 analysis shows important variations in spatiotemporal connectivity between these high elevation
553 zones and inflow to the basin which illustrate a heterogenous and compartmentalized regional
554 flow regime. The results of HYSPLIT back trajectories and our understanding of the modern
555 climate regime show that differences in initial atmospheric source in recharge and discharge
556 zones are not significant and cannot explain the substantial differences in isotopic signature we
557 observe between inflow and recharge. Ultimately, meteoric water in the system is derived almost
558 entirely from the Amazon and Chaco basins to the east, as this moisture traverses the Andean
559 plateau it undergoes substantial rainout and recycling fractionation. Average isotopic
560 composition of meteoric waters in each zone and their associated groundwaters reflect the
561 orientation of their respective recharge areas in relation to the dominant moisture sources and
562 topographic barriers they interact with. Specifically, the 1-1.2‰ enrichment in $\delta^{18}\text{O}$ observed in
563 waters discharging from the NE zone relative to the SE zone is due in part to the lack of rainout
564 fractionation in precipitation reaching its major recharge areas and the fact that the NE Divide
565 zone is on average ~250m lower in elevation than the SE Divide. With estimated $\delta^{18}\text{O}$ lapse rates
566 for this region between 0.9‰ and 1.7‰ per km of elevation (Rohrman et al., 2014), the
567 difference in recharge elevation could account for only about 0.2-0.4‰ of this enrichment. The
568 very prominent topographic barrier that exists to the east of the Miñiques and Miscanti lakes
569 (controlled by the COT fault system) may lead to consistent further isotopic depletion of
570 precipitation in the SE zone contributing areas (Figure 8) (Pingel et al., 2019). This is also
571 reflected in the nearly 2.0‰ enrichment in $\delta^{18}\text{O}$ seen in the NE Divide waters relative to SE
572 Divide waters.

573 The influence of snowmelt on groundwater recharge has been discussed as an important
574 control on the isotopic signature of groundwater in this region (Herrera et al., 2016). We argue
575 that since there are no permanent or deep snowfields in the entire region, snowfall is distributed

576 quite uniformly across the high altitudes and likely 20-30% of the snow is sublimated before
577 infiltrating, the signal of this snowmelt would not lead to systematic differences between recharge
578 zones or inflow zones not already discussed herein (Beria et al., 2018; Stigter et al., 2018; Vuille
579 & Ammann, 1997). In addition, the dominant moisture source and general climate regime is not
580 believed to have changed substantially through multiple pluvial periods during and since the last
581 glacial maximum, it's likely it was simply more amplified (Godfrey et al., 2003). This suggests
582 that the background precipitation signature we see in each of these zones due to orographic
583 effects and moisture source likely have not varied substantially through multiple pluvial periods.
584 However, it would be expected that the isotopic signature of this pluvial recharge would have a
585 distinct isotopic signal which can be identified in this dataset.

586 The water stable isotope data presented here consistently align parallel to but below the
587 LMWL and GMWL in $\delta^{18}\text{O}$ - $\delta^2\text{H}$ space, indicating another important and consistent distinction
588 between modern meteoric water and groundwater. A similar signal has been identified in the
589 Central Andes and in other arid regions for which two explanations have been proposed: the
590 continued evaporation of water during infiltration through the unsaturated zone (Barnes &
591 Walker, 1989; Fontes & Molinari, 1975; Zimmerman et al., 1967) and a direct signature of
592 pluvial groundwater recharge (Fritz et al., 1981; Magaritz et al., 1989; Meijer & Kwicklis, 2000).
593 Laboratory and field measurements of diffuse recharge in arid environments estimate that d-excess
594 excursions in groundwater recharge can range between -0‰ to as much as -10‰ relative to the
595 initial meteoric water (Barnes & Allison, 1988; DePaolo et al., 2004). In this region it is likely
596 that the actual influence of this process is somewhat less than the maximum due to the fact that
597 much of the recharge occurring in these arid mountains regions is focused (i.e. through fractures
598 and permeability contrasts) not diffuse in nature, heavily biased to larger precipitation events and
599 occurs at very high elevation with steeper LEL slopes than other arid environments. Recharge
600 waters from wetter periods in the past would fall along a different GMWL than the modern due to
601 differences in composition of the global ocean and the substantially higher relative humidity in
602 this region (Meijer & Kwicklis, 2000). This paleo-meteoric water line during the most recent
603 pluvial periods for instance is predicted to have a y-intercept of between 0 and 5, resulting in a d-
604 excess excursion from the LMWL of between -10‰ and -15‰ (Clark & Fritz, 1997; Fritz et al.
605 1981). The observed excursion (lc-excess) in the SE and NE zone groundwaters and spring
606 waters show an average of -10‰, the South zone -19‰ and high elevation waters -16‰
607 (Landwehr & Coplen, 2006). While both of these processes likely have some influence on these
608 observed isotopic shifts, the magnitude of the shift we document suggests that only a portion of
609 this signal can be accounted for with vadose zone fractionation. We argue that this signature has

610 a fingerprint of pluvial period groundwater recharge now draining from storage. A similar
611 signature has been identified in groundwater isotope data in arid regions worldwide where large
612 water and solute balances have also been observed, this may indicate the relative influence of
613 draining paleo-recharge and help explain these hydrological imbalances.

614 Stable isotope data from the South zone and the plateau zones appear to be skewed
615 further off the LMWL (illustrated by their large lc -excess) giving these waters an apparent LEL
616 slope shallower than would be expected (Figure 5). Additional isotopic fractionation caused by
617 isotopic exchange from interactions between silica-rich rock and high temperature fluids has been
618 documented in this and other regions with high tectonic activity, tending to evolve waters along a
619 nearly horizontal slope in $\delta^2H - \delta^{18}O$ space (Cortecci et al., 2005; Rissmann et al., 2015). Thermal
620 waters from two active sites in the El Tatio geothermal field, northern Chile (Cortecci et al.,
621 2005) and Jujuy Province on the northern Puna plateau of Argentina (Peralta Arnold et al., 2016)
622 provide approximate end-members with which to identify this influence (Figure 5). This shift
623 superimposed on the data is apparent in the plateau and South zone waters by the considerable
624 skew from the LMWL towards this geothermal end-member. This process may help explain some
625 of the apparent isotopic distinctions seen in the South zone waters with respect to the other inflow
626 zones. Waters discharging in the South may in fact be more similar to the SE waters in source but
627 are further fractionated as they flow towards the basin by the remnant heat from the Socompa
628 volcano, as indicted by Rissmann et al. (2015).

629 This work describes a large-scale integrated groundwater system where water is
630 transported over long time-scales and across a vast regional catchment, therefore it is also likely
631 that groundwater discharging to the SdA basin is connected to some degree with the many
632 internally drained sub-basins at high elevation (Figure 8). This solute-rich interbasin flow has
633 been suggested by Grosjean et al. (1995), Munk et al. (2018) and Rissmann et al. (2015) among
634 others as an important source of solutes to the SdA basin and explain in large part, the excess
635 mass accumulated in the evaporite deposit. Three pieces of evidence in our results support this
636 interpretation: (i) the regions we call the Divide zones, straddling the SdA watershed divide have
637 water isotope signatures that are consistent with groundwater discharge to the SdA and therefore
638 also consistent with infiltration occurring within these perched watersheds; (ii) the density of
639 active salars and salt lakes close to the watershed divide, bounded to the north by the COT fault
640 system is much higher than in the northern half of the basin; and (iii) the waters in the South and
641 SE zone have much higher concentrations of conservative solutes than other parts of the basin as
642 discussed by Munk et al. (2018).

643 **6. Conclusions**

644 Our exhaustive examination of isotopic systematics in the orogenic-scale groundwater
645 system manifest at SdA constrains the sources of water and flow paths entering the basin and
646 demonstrates that modern water inputs in the system are limited and focused. We define the
647 dimensions of paleo-recharge water and connections among water bodies in the basin and on the
648 plateau, illustrating fundamental governing mechanisms of the regional system. We offer
649 compelling evidence that investigations of water use and sustainability in this region must
650 integrate modern observations with an understanding of processes operating on very large spatial
651 and temporal scales. As an archetype of arid continental basins worldwide, these mechanisms, to
652 varying degrees are critical for reconciling observed imbalances and must be spatiotemporally
653 constrained in any model representing these systems. This work provides a framework within
654 which to identify these mechanisms and connections at the catchment scale thereby allowing
655 water resources to be more responsibly developed worldwide.

656 **7. Acknowledgements**

657 The authors want to thank Scott Hynek for the extensive advice and consultation he
658 provided on this work, it greatly improved the clarity of this manuscript; and Linda Godfrey for
659 providing valuable unpublished data to fill gaps in our dataset. We would also like to
660 acknowledge Albemarle Corp. for their continued support of this and related research to improve
661 the fundamental understanding of the hydrogeology and geochemistry of the SdA environment.
662 We are grateful for their permission to publish geochemical data relevant to this manuscript. The
663 ASTER DEM and Landsat 8 OLI were retrieved from EarthExplorer, courtesy of the NASA Land
664 Processes Distributed Active Archive Center, USGS/Earth Resources Observation and Science
665 Center. The data used in this work will be made available on the WaterIsotopes Database
666 (<http://wateriso.utah.edu/waterisotopes.html>).

667 **Figure Captions:**

668 **Figure 2.** Shaded relief digital elevation model of the Central Andes. Salars, lagoons and major
669 drainages (quebradas and rivers) are light blue. Topographic watersheds of major basins are
670 outlined in black. Extent of the Preandean Depression and Altiplano/Puna plateau are outlined
671 in white dashes. Isohyetal contours with associated values are dark blue dashed lines. Locations
672 of generalized geologic cross-sections in Figure S1 are red. Red dots are precipitation gauges
673 and sites used for HYSPLIT models. MNT Trough structure is shaded.

674 **Figure 2.** The SdA topographic watershed (solid black line), its recharge zones (black dashed
675 ellipses) and discharge/inflow zones (solid colored lines). Dots represent sample sites, grouped
676 by water type. Discharge zones extend from the salar margin to 4000 mamsl. Major drainages

677 (quebradas and rivers) are shown in white and salars and lagoons in light blue and dark blue
678 respectively. Notable high elevation lagoons Miñiques, Miscanti and Lejía are labeled. Surface
679 expression of the Peine/Cas structure is hatched.

680 **Figure 3.** Modern water content in samples (n=87) proportional to circle size. Shaded areas are
681 inflow water zones. Data from Grosjean et al. (1995) are orange. Circles in Nucleus and
682 Transition Zone represent average of water groupings. Surface waters (sw) are outlined in red,
683 groundwaters (gw) in blue.

684 **Figure 4. (a)** Modern water proportion (R_{mod}) among groundwater and surface water bodies
685 along transect of eastern SdA margin. South Inflow and East Inflow waters are averaged as a
686 single low elevation inflow water body. Mean R_{mod} value of each water grouping (in black
687 rectangles) and mean Specific Conductivity (SC) in mS/cm. **(b)** Tukey box plot of 3H content (TU)
688 in these water bodies. Blue dashed line is the theoretical maximum limit (0.15TU) of background
689 3H produced in-situ water-rock interaction.

690 **Figure 5.** All water stable isotope data from the SdA regional watershed (n=889). Colors
691 correspond to the three inflow zones labeled in Figure 2, brown points are all plateau waters.
692 Meteoric source water isotopic signature is estimated for each zone where LEL intersects the
693 Local Meteoric Water line (LMWL) of Chaffaut et al. (1998). High temperature waters from the
694 El Tatio thermal field and northern Puna region indicated by red Xs.

695 **Figure 6.** All stable water isotope data from plateau and divide recharge zones. Inflow waters
696 (NE and SE zones) are red and blue points displayed for context with inflow. Predicted meteoric
697 source waters from LEL intercept with LMWL are colored numbers.

698 **Figure 7.** $\delta^{18}O$ in waters from each zone plotted against sample elevation. Recharge limit line
699 denotes elevation below which no significant recharge occurs. Blue shaded envelope represents
700 the salar evaporite aquifer below the basin floor. Specific Conductivity ($\mu S/cm$) of sample
701 groupings in italics. Ellipses in **(a)**, **(b)** and **(c)** indicate descriptive groupings discussed in text and
702 blue arrows indicate general hydrochemical evolutionary pathways. Dashed slope in **(d)**
703 indicates predicted trend of isotopic evolution. Water types and locations are labeled in legend
704 (Spr.=Spring water).

705 **Figure 8.** Conceptual model of integrated SdA regional groundwater system. Major mechanisms
706 governing the contemporary hydrologic system and their relative influence. Shown in plan view
707 **(a)**, solid light blue arrows represent the distribution of modern meteoric inputs and their
708 signatures, brown dashed line denotes a major orographic barrier to precipitation east of
709 Miñiques and Miscanti lakes. Solid blue arrows represent inflows of modern recharge, green
710 dashed arrows are major inputs of paleo-groundwater, red dashed arrows show hypothesized
711 influx of solute-rich fluid. **(b)** Cross-sectional view of the SE zone shows the distribution and
712 relative importance of these hydrological mechanisms. Blue lines are the estimated position of
713 the modern water table, green is the LGM water table and the corresponding flow paths of
714 modern and paleo-groundwater, red is solute-rich influx.

715 **Table Captions:**

716 **Table 1.** 3H data from waters collected in this study and from Grosjean et al., 1995. Column 3H
717 contains analytical results, *Error* the analytical error associated with each analysis, $^3H^*$ is the 3H
718 value decayed to a common date and $R_{mod\#}$ is the relative ratio of modern water in each sample.

719 **Table 2.** Calculations of transit time estimates assuming piston flow and a decay constant. High
 720 elevation lake water ^3H value and modern meteoric water are used as input water ^3H values.
 721 These input ^3H values were decayed and seepage velocities (v) estimated with aquifer properties
 722 (K & θ) from Houston (2007) and a plausible range of values. Velocities calculated by piston flow
 723 transit times, then MRT of waters estimated under these conditions.

724

725 **References**

726

- 727 Allmendinger, R. W., Jordan, T. E., Kay, S. M., & Isacks, B. L. (1997). The Evolution of The
 728 Altiplano-Puna Plateau of the Central Andes. *Annual Review of Earth and Planetary*
 729 *Sciences*, 25(1), 139–174. <https://doi.org/10.1146/annurev.earth.25.1.139>
- 730 Ammann, C., Jenny, B., Kammer, K., & Messerli, B. (2001). Late quaternary glacier response to
 731 humidity changes in the arid Andes of Chile (18-29°S). *Palaeogeography,*
 732 *Palaeoclimatology, Palaeoecology*, 172(3–4), 313–326. [https://doi.org/10.1016/S0031-](https://doi.org/10.1016/S0031-0182(01)00306-6)
 733 [0182\(01\)00306-6](https://doi.org/10.1016/S0031-0182(01)00306-6)
- 734 Aravena, R. (1995). Isotope hydrology and geochemistry of northern Chile groundwaters.
 735 *Bulletin - Institut Francais d'Etudes Andines*, 24(3), 495–503.
- 736 Aravena, R., Suzuki, O., Peña, H., Pollastri, a., Fuenzalida, H., & Grilli, a. (1999). Isotopic
 737 composition and origin of the precipitation in Northern Chile. *Applied Geochemistry*,
 738 14(4), 411–422. [https://doi.org/10.1016/S0883-2927\(98\)00067-5](https://doi.org/10.1016/S0883-2927(98)00067-5)
- 739 Aron, F., González, G., Veloso, E., & Cembrano, J. (2008). Architecture and style of compressive
 740 Neogene deformation in the eastern-southeastern border of the Salar de Atacama Basin
 741 (22 30' -24 15'S): A structural setting for the active volcanic arc of the Central Andes. In
 742 7th International Symposium on Andean Geodynamics (ISAG 2008, Nice) (pp. 52-55)
- 743 Barnes, C. J., & Allison, G. B. (1988). Tracing of water movement in the unsaturated zone using
 744 stable isotopes of hydrogen and oxygen. *Journal of Hydrology*, 100(1–3), 143–176.
 745 [https://doi.org/10.1016/0022-1694\(88\)90184-9](https://doi.org/10.1016/0022-1694(88)90184-9)
- 746 Barnes, C. J., & Walker, G. R. (1989). The distribution of deuterium and oxygen-18 during
 747 unsteady evaporation from a dry soil. *Journal of Hydrology*, 112(1–2), 55–67.
 748 [https://doi.org/10.1016/0022-1694\(89\)90180-7](https://doi.org/10.1016/0022-1694(89)90180-7)
- 749 Belcher, W. R., Bedinger, M. S., Back, J. T., & Sweetkind, D. S. (2009). Interbasin flow in the
 750 Great Basin with special reference to the southern Funeral Mountains and the source of
 751 Furnace Creek springs, Death Valley, California, U.S. *Journal of Hydrology*, 369(1–2),
 752 30–43. <https://doi.org/10.1016/j.jhydrol.2009.02.048>
- 753 Bershaw, J., S. M. Penny, and C. N. Garziona (2012). Stable isotopes of modern water across the
 754 Himalaya and eastern Tibetan Plateau: Implications for estimates of paleoelevation and
 755 paleoclimate, *J. Geophysical. Research*, 117, D02110, doi:10.1029/2011JD016132
- 756 Betancourt, J. L., Latorre, C., Rech, J. A., Quade, J., & Rylander, K. A. (2000). A 22,000-year
 757 record of monsoonal precipitation from northern Chile's Atacama Desert. *Science*,
 758 289(5484), 1542-1546
- 759 Beria, H., Larsen, J. R., Ceperley, N. C., Michelon, A., Vennemann, T., & Schaepli, B. (2018).
 760 Understanding snow hydrological processes through the lens of stable water isotopes.
 761 *Wiley Interdisciplinary Reviews: Water*, 5(6), e1311. <https://doi.org/10.1002/wat2.1311>
- 762 Blard, P. H., Sylvestre, F., Tripathi, A. K., Claude, C., Causse, C., Coudrain, A., ... Lavé, J.
 763 (2011). Lake highstands on the Altiplano (Tropical Andes) contemporaneous with
 764 Heinrich 1 and the Younger Dryas: New insights from ^{14}C , U-Th dating and $\delta^{18}\text{O}$ of
 765 carbonates. *Quaternary Science Reviews*, 30(27–28), 3973–3989.
 766 <https://doi.org/10.1016/j.quascirev.2011.11.001>

- 767 Blodgett, T. a., J. D. Lenters, and B. L. Isacks (1997). Constraints on the origin of paleolake
768 expansions in the Central Andes, *Earth Interact.*, 1(1), 1–1, doi:10.1175/1087-
769 3562(1997)001<0001: CotOoP>2.0.CO;2
- 770 Bobst, A. L., Lowenstein, T. K., Jordan, T. E., Godfrey, L. V., Ku, T. L., & Luo, S. (2001). A 106
771 ka paleoclimate record from drill core of the Salar de Atacama, northern Chile.
772 *Palaeogeography, Palaeoclimatology, Palaeoecology*, 173(1–2), 21–42.
773 [https://doi.org/10.1016/S0031-0182\(01\)00308-X](https://doi.org/10.1016/S0031-0182(01)00308-X)
- 774 Boers, N., Bookhagen, B., Marwan, N., & Kurths, J. (2016). Spatiotemporal characteristics and
775 synchronization of extreme rainfall in South America with focus on the Andes Mountain
776 range. *Climate dynamics*, 46(1-2), 601-617
- 777 Boschetti, T., Cortecchi, G., Barbieri, M., & Mussi, M. (2007). New and past geochemical data on
778 fresh to brine waters of the Salar de Atacama and Andean Altiplano, northern Chile.
779 *Geofluids*, 7(1), 33-50.
- 780 Boschetti, Cifuentes, Iacumin, & Selmo. (2019). Local Meteoric Water Line of Northern Chile
781 (18° S–30° S): An Application of Error-in-Variables Regression to the Oxygen and
782 Hydrogen Stable Isotope Ratio of Precipitation. *Water*, 11(4), 791.
783 doi:10.3390/w11040791
- 784 Boutt, D. F., Hynek, S. A., Munk, L. A., & Corenthal, L. G. (2016). Rapid recharge of fresh water
785 to the halite-hosted brine aquifer of Salar de Atacama, Chile. *Hydrological Processes*,
786 30(25), 4720–4740. <https://doi.org/10.1002/hyp.10994>
- 787 Boutt, D., Corenthal, L., Munk, L. A., & Hynek, S. (2018). Imbalance in the modern hydrologic
788 budget of topographic catchments along the western slope of the Andes (21–25 S).
789 <https://doi.org/10.31223/osf.io/p5tsq>
- 790 Breitkreuz, C. (1995). The late Permian Peine and Cas Formations at the eastern margin of the
791 Salar de Atacama, Northern Chile: stratigraphy, volcanic facies, and tectonics. *Revista*
792 *Geológica de Chile*, 22(1), 3–23.
- 793 Burg, A., Zilberbrand, M., & Yechieli, Y. (2013). Radiocarbon Variability in Groundwater in an
794 Extremely Arid Zone—The Arava Valley, Israel. *Radiocarbon*, 55(2), 963–978.
795 <https://doi.org/10.1017/s0033822200058112>
- 796 Cartwright, I., Cendón, D., Currell, M., & Meredith, K. (2017). A review of radioactive isotopes
797 and other residence time tracers in understanding groundwater recharge: Possibilities,
798 challenges, and limitations. *Journal of Hydrology*, 555, 797–811.
799 <https://doi.org/10.1016/j.jhydrol.2017.10.053>
- 800 Cervetto Sepúlveda, M. M. (2012). Caracterización hidrogeológica e hidrogeoquímica de las
801 cuencas: Salar de Aguas calientes 2, Puntas negras, Laguna Tuyajto, Pampa Colorada,
802 Pampa Las Tecas y Salar el Laco, II región de Chile.
- 803 Chaffaut I, Coudrain-Ribstein A, Michelot JL, Pouyaud B. (1998) Precipitations d’altitude du
804 Nord-Chili, origine des sources de vapeur et donnees isotopiques. *Bulletin de l’Institute*
805 *Francais d etudes andine*, 27, 367–84.
- 806 Clark, I. D. 1., & Fritz, P. 1. (1997). *Environmental isotopes in hydrogeology*. Boca Raton, FL:
807 CRC Press/Lewis Publishers.
- 808 Clarke, W.B., Jenkins, W.J., Top, Z. (1976). Determination of Tritium by Mass Spectrometric
809 Measurement of ³He. *International Journal of Applied Radiation and Isotopes* 27, 515–
810 522.
- 811 Cook PG, Bohlke J-K. (2000). Determining timescales for groundwater flow and solute transport.
812 In *Environmental Tracers in Subsurface Hydrology*, Cook PG, Herczeg AL (eds). Kluwer
813 Academic Publishers: Norwell, MA; 1–30.
- 814 Corenthal, L. G., Boutt, D. F., Hynek, S. A., & Munk, L. A. (2016). Regional groundwater flow
815 and accumulation of a massive evaporite deposit at the margin of the Chilean Altiplano.
816 *Geophysical Research Letters*, 43(15), 8017–8025. <https://doi.org/10.1002/2016GL070076>

- 817 Cortecchi, G., Boschetti, T., Mussi, M., Lameli, C. H., Mucchino, C., & Barbieri, M. (2005). New
 818 chemical and original isotopic data on waters from El Tatio geothermal field, northern
 819 Chile. *Geochemical Journal*, 39(6), 547–571. <https://doi.org/10.2343/geochemj.39.547>
 820 Currell, M., Gleeson, T., Dahlhaus, P. (2016). A New Assessment Framework for Transience in
 821 Hydrogeological Systems. *Groundwater* 54, 4–14. doi:10.1111/gwat.12300
 822 DePaolo, D. J., M. E. Conrad, K. Maher, and G. W. Gee. 2004. Evaporation Effects on Oxygen
 823 and Hydrogen Isotopes in Deep Vadose Zone Pore Fluids at Hanford, Washington.
 824 *Vadose Zone J.* 3:220-232. doi:10.2136/vzj2004.2200
 825 De Porras, M. E., Maldonado, A., De Pol-Holz, R., Latorre, C., & Betancourt, J. L. (2017). Late
 826 Quaternary environmental dynamics in the Atacama Desert reconstructed from rodent
 827 midden pollen records. *Journal of Quaternary Science*, 32(6), 665–684.
 828 <https://doi.org/10.1002/jqs.2980>
 829 DGA [Dirección General de Aguas] (2013), Análisis de la Oferta Hídrica del Salar de Atacama,
 830 Santiago, Chile.
 831 Draxler, R. R., & G. D. Hess (1998). An overview of the HYSPLIT_4 modelling system for
 832 trajectories, dispersion and deposition, *Aust. Meteorol. Mag.*, 47(4), 295–308.
 833 Eugster, H. P. (1980). Geochemistry of evaporitic lacustrine deposits. *Annual Review of Earth
 834 and Planetary Sciences: Volume 8*, 35–63.
 835 Favreau, G., Cappelaere, B., Massuel, S., Leblanc, M., Boucher, M., Boulain, N., & Leduc, C.
 836 (2009). Land clearing, climate variability, and water resources increase in semiarid
 837 southwest Niger: A review. *Water Resources Research*, 45(7).
 838 <https://doi.org/10.1029/2007WR006785>
 839 Fiorella, R. P., Poulsen, C. J., Pillco Zolá, R. S., Barnes, J. B., Tabor, C. R., & Ehlers, T. A.
 840 (2015). Spatiotemporal variability of modern precipitation $\delta^{18}\text{O}$ in the central Andes and
 841 implications for paleoclimate and paleoaltimetry estimates. *Journal of Geophysical
 842 Research*, 120(10), 4630–4656. <https://doi.org/10.1002/2014JD022893>
 843 Fontes, J C, & Molinari, J. (1975). Isotopic study of the upper watershed of the Rio Abancan
 844 (Province of Catamarca, Argentina). *Rev. Geogr. Phys. Geol. Dyn.; (France); Journal
 845 Volume: 7:5*
 846 Fritz, P., Silva, H., Suzuki, O., & Salati, E. (1979). Isotope hydrology in northern Chile. In
 847 *Isotope hydrology 1978*.
 848 Fritz, P., Suzuki, O., Silva, C., & Salati, E. (1981). Isotope hydrology of groundwaters in the
 849 Pampa del Tamarugal, Chile. *Journal of Hydrology*, 53(1–2), 161–184.
 850 [https://doi.org/10.1016/0022-1694\(81\)90043-3](https://doi.org/10.1016/0022-1694(81)90043-3)
 851 Fritz, S. C., P. a. Baker, T. K. Lowenstein, G. O. Seltzer, C. a. Rigsby, G. S. Dwyer, P. M. Tapia,
 852 K. K. Arnold, T. L. Ku, and S. Luo (2004). Hydrologic variation during the last 170,000
 853 years in the southern hemisphere tropics of South America, *Quat. Res.*, 61(1), 95–104.
 854 doi: 10.1016/j.yqres.2003.08.007
 855 Gardeweg, M., & Ramírez, C. F. (1987). La Pacana caldera and the Atana Ignimbrite - a major
 856 ash-flow and resurgent caldera complex in the Andes of northern Chile. *Bulletin of
 857 Volcanology*, 49(3), 547–566. <https://doi.org/10.1007/BF01080449>
 858 Garreaud, R., M. Vuille, & A. C. Clement (2003). The climate of the Altiplano: Observed current
 859 conditions and mechanisms of past changes, *Palaeogeography, Palaeoclimatology,
 860 Palaeoecology.*, 194(1-3), 5–22, doi:10.1016/S0031-0182(03)00269-4.
 861 Garreaud, R. D. (2009). The Andes climate and weather. *Advances in Geosciences*, 22, 3–11.
 862 <https://doi.org/10.5194/adgeo-22-3-2009>
 863 Gasse, F. (2000). Hydrological changes in the African tropics since the Last Glacial Maximum. In
 864 *Quaternary Science Reviews (Vol. 19, pp. 189–211)*. [https://doi.org/10.1016/S0277-3791\(99\)00061-X](https://doi.org/10.1016/S0277-3791(99)00061-X)
 865
 866 Ge, J., Chen, J., Ge, L., Wang, T., Wang, C., & Chen, Y. (2016). Isotopic and hydrochemical
 867 evidence of groundwater recharge in the Hopq Desert, NW China. *Journal of*

- 868 Radioanalytical and Nuclear Chemistry, 310(2), 761–775. [https://doi.org/10.1007/s10967-](https://doi.org/10.1007/s10967-016-4856-8)
869 016-4856-8
- 870 Gleeson, T., L. Marklund, L. Smith, and A. H. Manning (2011), Classifying the water table at
871 regional to continental scales, *Geophys. Res. Lett.*, 38, L05401, doi:10.1029/
872 2010GL046427.
- 873 Gleeson, T., Wada, Y., Bierkens, M.F.P., van Beek, L.P.H., (2012). Water balance of global
874 aquifers revealed by groundwater footprint. *Nature* 488, 197–200.
875 doi:10.1038/nature11295
- 876 Godfrey, L. V., Jordan, T. E., Lowenstein, T. K., & Alonso, R. L. (2003). Stable isotope
877 constraints on the transport of water to the Andes between 22° and 26°S during the last
878 glacial cycle. In *Palaeogeography, Palaeoclimatology, Palaeoecology* (Vol. 194, pp. 299–
879 317). Elsevier B.V. [https://doi.org/10.1016/S0031-0182\(03\)00283-9](https://doi.org/10.1016/S0031-0182(03)00283-9)
- 880 González, G., Cembrano, J., Aron, F., Veloso, E. E., & Shyu, J. B. H. (2009). Coeval
881 compressional deformation and volcanism in the central Andes, case studies from northern
882 Chile (23°S–24°S). *Tectonics*, 28(6). <https://doi.org/10.1029/2009TC002538>
- 883 Grosjean, M., Geyh, M. A., Messerli, B., & Schotterer, U. (1995). Late-glacial and early
884 Holocene lake sediments, ground-water formation and climate in the Atacama Altiplano
885 22–24°S. *Journal of Paleolimnology*, 14(3), 241–252.
886 <https://doi.org/10.1007/BF00682426>.
- 887 Hartley, A. J., and G. Chong (2002), Late Pliocene age for the Atacama Desert: Implications for
888 the desertification of western South America, *Geology*, 30(1), 43–46, doi:10.1130/0091-
889 7613(2002)030<0043: LPAFTA>2.0.CO;2
- 890 Haitjema, H. M., & S. Mitchell-Bruker (2005), Are water tables a subdued replica of the
891 topography? *Ground Water*, 43, 781–786.
- 892 Herrera, C., Custodio, E., Chong, G., Lambán, L. J., Riquelme, R., Wilke, H., ... Lictevoid, E.
893 (2016). Groundwater flow in a closed basin with a saline shallow lake in a volcanic area:
894 Laguna Tuyajto, northern Chilean Altiplano of the Andes. *Science of the Total*
895 *Environment*, 541, 303–318. <https://doi.org/10.1016/j.scitotenv.2015.09.060>
- 896 Houston, J. (2002). Groundwater recharge through an alluvial fan in the Atacama Desert,
897 northern Chile: mechanisms, magnitudes and causes. *Hydrological processes*, 16(15),
898 3019–3035.
- 899 Houston, J. (2006a). The great Atacama flood of 2001 and its implications for Andean hydrology.
900 *Hydrological Processes*, 20(3), 591–610. <https://doi.org/10.1002/hyp.5926>
- 901 Houston, J. (2006b). Variability of precipitation in the Atacama Desert: its causes and
902 hydrological impact. *International Journal of Climatology*, 26(15), 2181–2198.
- 903 Houston, J. (2007). Recharge to groundwater in the Turi Basin, northern Chile: An evaluation
904 based on tritium and chloride mass balance techniques. *Journal of Hydrology*, 334(3–4),
905 534–544. <https://doi.org/10.1016/j.jhydrol.2006.10.030>
- 906 Houston, J. (2009). A recharge model for high altitude, arid, Andean aquifers. *Hydrological*
907 *Processes*, 23(16), 2383–2393. <https://doi.org/10.1002/hyp.7350>
- 908 Houston, J. & Hart, D. (2004). Theoretical head decay in closed basin aquifers: an insight into
909 fossil groundwater and recharge events in the Andes of northern Chile. *Quarterly Journal*
910 *of Engineering Geology and Hydrogeology* 37, 131–139. doi:10.1144/1470-9236/04-007
- 911 Jasechko, S. (2016). Partitioning young and old groundwater with geochemical tracers. *Chemical*
912 *Geology*, 427, 35–42. <https://doi.org/10.1016/j.chemgeo.2016.02.012>
- 913 Jasechko, S., S. J. Birks, T. Gleeson, Y. Wada, P. J. Fawcett, Z. D. Sharp, J. J. McDonnell, and J.
914 M. Welker (2014), The pronounced seasonality of global groundwater recharge, *Water*
915 *Resour. Res.*, 50, 8845–8867, doi:10.1002/2014WR015809
- 916 Jasechko, S., Perrone, D., Befus, K. M., Bayani Cardenas, M., Ferguson, G., Gleeson, T., ...
917 Kirchner, J. W. (2017). Global aquifers dominated by fossil groundwaters but wells

- 918 vulnerable to modern contamination. *Nature Geoscience*, 10(6), 425–429.
919 <https://doi.org/10.1038/ngeo2943>
- 920 Jordan, T. E., L. V. Godfrey, N. Munoz, R. N. Alonso, T. K. Lowenstein, G. D. Hoke, N.
921 Peranginangin, B. L. Isacks, and L. Cathles (2002), Orogenic-scale ground water
922 circulation in the Central Andes: evidence and consequences., 5th ISAG (International
923 Symp. Andean Geodyn., 331–334.
- 924 Jordan, T. E., Nester, P. L., Blanco, N., Hoke, G. D., Dávila, F., & Tomlinson, A. J. (2010).
925 Uplift of the Altiplano-Puna plateau: A view from the west. *Tectonics*, 29(5).
926 <https://doi.org/10.1029/2010TC002661>
- 927 Jordan, T., Lameli, C. H., Kirk-Lawlor, N., & Godfrey, L. (2015). Architecture of the aquifers of
928 the Calama Basin, Loa catchment basin, northern Chile. *Geosphere*, 11(5), 1438–1474.
929 <https://doi.org/10.1130/GES01176.1>
- 930 Jordan, T. E., Herrera L., C., Godfrey, L. V., Colucci, S. J., Gamboa P., C., Urrutia M., J., ...
931 Paul, J. F. (2019). Isotopic characteristics and paleoclimate implications of the extreme
932 precipitation event of march 2015 in Northern Chile. *Andean Geology*, 46(1), 1–31.
933 <https://doi.org/10.5027/andgeov46n1-3087>
- 934 Kafri, U., & Yechieli, Y. (2012). The relationship between current and paleo groundwater base-
935 levels. *Quaternary International*, 257, 83–96. <https://doi.org/10.1016/j.quaint.2011.08.028>
- 936 Kampf, S. K., & Tyler, S. W. (2006). Spatial characterization of land surface energy fluxes and
937 uncertainty estimation at the Salar de Atacama, Northern Chile. *Advances in Water
938 Resources*, 29(2), 336–354. <https://doi.org/10.1016/j.advwatres.2005.02.017>
- 939 Kendall, C., & Caldwell, E. A. (1998). Fundamentals of Isotope Geochemistry. In *Isotope Tracers
940 in Catchment Hydrology* (pp. 51–86). Elsevier. [https://doi.org/10.1016/b978-0-444-
941 81546-0.50009-4](https://doi.org/10.1016/b978-0-444-81546-0.50009-4)
- 942 Kendall, C., & McDonnell, J. J. (1998). *Isotope tracers in catchment hydrology*. Isotope tracers in
943 catchment hydrology. Elsevier Science B.V.
- 944 Kirchner, J. W. (2006). Getting the right answers for the right reasons: Linking measurements,
945 analyses, and models to advance the science of hydrology. *Water Resources Research*,
946 42(3). <https://doi.org/10.1029/2005WR004362>
- 947 Koeniger, P., Gaj, M., Beyer, M., & Himmelsbach, T. (2016). Review on soil water isotope-based
948 groundwater recharge estimations. *Hydrological Processes*, 30(16), 2817–2834.
949 <https://doi.org/10.1002/hyp.10775>
- 950 Kröpelin, S., Verschuren, D., Lézine, A. M., Eggermont, H., Cocquyt, C., Francus, P., ...
951 Engstrom, D. R. (2008). Climate-driven ecosystem succession in the Sahara: The past
952 6000 years. *Science*, 320(5877), 765–768. <https://doi.org/10.1126/science.1154913>
- 953 Langenbrunner, B., Pritchard, M. S., Kooperman, G. J., & Randerson, J. T. (2019). Why Does
954 Amazon Precipitation Decrease When Tropical Forests Respond to Increasing CO₂?
955 *Earth's Future*, 7(4), 450–468. <https://doi.org/10.1029/2018EF001026>
- 956 Landwehr, J. M., & Coplen, T. B. (2006). Line-conditioned excess: a new method for
957 characterizing stable hydrogen and oxygen isotope ratios in hydrologic systems.
958 *International conference on isotopes in environmental studies* (pp. 132–135).
- 959 Latorre, C., Betancourt, J. L., Rylander, K. A., Quade, J., & Matthei, O. (2003). A vegetation
960 history from the arid prepuna of northern Chile (22–23°S) over the last 13 500 years. In
961 *Palaeogeography, Palaeoclimatology, Palaeoecology* (Vol. 194, pp. 223–246). Elsevier
962 B.V. [https://doi.org/10.1016/S0031-0182\(03\)00279-7](https://doi.org/10.1016/S0031-0182(03)00279-7)
- 963 Lindsey, B.D., Jurgens, B.C., and Belitz, K. (2019). Tritium as an indicator of modern, mixed,
964 and premodern groundwater age: U.S. Geological Survey Scientific Investigations Report
965 2019–5090, 18 p., <https://doi.org/10.3133/sir20195090>
- 966 Love, A. H., & Zdon, A. (2018). Use of radiocarbon ages to narrow groundwater recharge
967 estimates in the southeastern Mojave Desert, USA. *Hydrology*, 5(3).
968 <https://doi.org/10.3390/hydrology5030051>

- 969 Lowenstein, T. K., Hein, M. C., Bobst, A. L., Jordan, T. E., Ku, T.-L., & Luo, S. (2003). An
970 Assessment of Stratigraphic Completeness in Climate-Sensitive Closed-Basin Lake
971 Sediments: Salar de Atacama, Chile. *Journal of Sedimentary Research*, 73(1), 91–104.
972 <https://doi.org/10.1306/061002730091>
- 973 Lucas, L.L., Unterweger (2000). Comprehensive Review and Critical Evaluation of the Half-Life
974 of Tritium. *Journal of Research of the National Institute of Standards and Technology* 105,
975 541–549.
- 976 Magaritz, M., Aravena, R., Peña, H., Suzuki, O., & Grilli, A. (1989). Water chemistry and isotope
977 study of streams and springs in northern Chile. *Journal of Hydrology*, 108(C), 323–341.
978 [https://doi.org/10.1016/0022-1694\(89\)90292-8](https://doi.org/10.1016/0022-1694(89)90292-8)
- 979 Magilligan, F. J., Goldstein, P. S., Fisher, G. B., Bostick, B. C., & Manners, R. B. (2008). Late
980 Quaternary hydroclimatology of a hyper-arid Andean watershed: Climate change, floods,
981 and hydrologic responses to the El Niño-Southern Oscillation in the Atacama Desert.
982 *Geomorphology*, 101(1–2), 14–32. <https://doi.org/10.1016/j.geomorph.2008.05.025>
- 983 Mather, A. E., & Hartley, A. (2005). Flow events on a hyper-arid alluvial fan: Quebrada
984 Tambores, Salar de Atacama, northern Chile. *Geological Society Special Publication*, 251,
985 9–24. <https://doi.org/10.1144/GSL.SP.2005.251.01.02>
- 986 Maxey, G. B. (1968). Hydrogeology of Desert Basins. *Groundwater*, 6(5), 10–22.
987 <https://doi.org/10.1111/j.1745-6584.1968.tb01660.x>
- 988 McKnight, Sarah, (2019). "The Climatic and Hydrostratigraphic Controls on Brine-to-Freshwater
989 Interface Dynamics in Hyperarid Climates: A 2-D Parametric Groundwater Modeling
990 Study". Masters Theses. 785. https://scholarworks.umass.edu/masters_theses_2/785
- 991 Meijer, A. & Kwicklis, E. (2000). Geochemical and Isotopic Constraints on Ground-Water Flow
992 Directions, Mixing and Recharge at Yucca Mountain, Nevada. United States.
993 doi:10.2172/883407
- 994 Müller, T., Osenbrück, K., Strauch, G., Pavetich, S., Al-Mashaikhi, K. S., Herb, C., ... Sanford,
995 W. (2016). Use of multiple age tracers to estimate groundwater residence times and long-
996 term recharge rates in arid southern Oman. *Applied Geochemistry*, 74, 67–83.
997 <https://doi.org/10.1016/j.apgeochem.2016.08.012>
- 998 Munk, L. A., Boutt, D. F., Hynek, S. A., & Moran, B. J. (2018). Hydrogeochemical fluxes and
999 processes contributing to the formation of lithium-enriched brines in a hyper-arid
1000 continental basin. *Chemical Geology*, 493, 37–57.
1001 <https://doi.org/10.1016/j.chemgeo.2018.05.013>
- 1002 Ortiz, C., Aravena, R., Briones, E., Suárez, F., Tore, C., & Muñoz, J. F. (2014). Sources of
1003 surface water for the Soncor ecosystem, Salar de Atacama basin, northern Chile.
1004 *Hydrological Sciences Journal*, 59(2), 336-350.
- 1005 Pascale, S., Carvalho, L. M. V., Adams, D. K., Castro, C. L., & Cavalcanti, I. F. A. (2019).
1006 Current and Future Variations of the Monsoons of the Americas in a Warming Climate.
1007 *Current Climate Change Reports*. Springer. <https://doi.org/10.1007/s40641-019-00135-w>
- 1008 Peralta Arnold, Y., Cabassi, J., Tassi, F., Caffè, P. J., & Vaselli, O. (2017). Fluid geochemistry of
1009 a deep-seated geothermal resource in the Puna plateau (Jujuy Province, Argentina).
1010 *Journal of Volcanology and Geothermal Research*, 338, 121–134.
1011 <https://doi.org/10.1016/j.jvolgeores.2017.03.030>
- 1012 Pérez-Fodich, A., Reich, M., Alvarez, F., Snyder, G. T., Schoenberg, R., Vargas, G., ... & Fehn,
1013 U. (2014). Climate change and tectonic uplift triggered the formation of the Atacama
1014 Desert's giant nitrate deposits. *Geology*, 42(3), 251-254.
- 1015 Pingel, H., Alonso, R. N., Altenberger, U., Cottle, J., & Strecker, M. R. (2019). Miocene to
1016 Quaternary basin evolution at the southeastern Andean Plateau (Puna) margin (ca. 24°S
1017 lat, Northwestern Argentina). *Basin Research*, 31(4), 808–826.
1018 <https://doi.org/10.1111/bre.12346>

- 1019 Placzek, C., Quade, J., & Patchett, P. J. (2006). Geochronology and stratigraphy of late
1020 Pleistocene lake cycles on the southern Bolivian Altiplano: Implications for causes of
1021 tropical climate change. *Bulletin of the Geological Society of America*, 118(5–6), 515–
1022 532. <https://doi.org/10.1130/B25770.1>
- 1023 Placzek, C., Quade, J., Betancourt, J. L., Patchett, P. J., Rech, J. A., Latorre, C., ... English, N. B.
1024 (2009). CLIMATE IN THE DRY CENTRAL ANDES OVER GEOLOGIC,
1025 MILLENNIAL, AND INTERANNUAL TIMESCALES. *Annals of the Missouri*
1026 *Botanical Garden*, 96(3), 386–397. <https://doi.org/10.3417/2008019>
- 1027 Placzek, C. J., Quade, J., & Patchett, P. J. (2013). A 130ka reconstruction of rainfall on the
1028 Bolivian Altiplano. *Earth and Planetary Science Letters*, 363, 97–108.
1029 <https://doi.org/10.1016/j.epsl.2012.12.017>
- 1030 Quade, J., Rech, J. A., Betancourt, J. L., Latorre, C., Quade, B., Rylander, K. A., & Fisher, T.
1031 (2008). Paleowetlands and regional climate change in the central Atacama Desert,
1032 northern Chile. *Quaternary Research*, 69(3), 343–360.
- 1033 Ramirez, C., and M. Gardeweg (1982). *Carta Geologica de Chile, escala 1:250000, Hoja*
1034 *Toconao, Region de Antofagasta, Chile No. 54, Santiago, Chile.*
- 1035 Rech, J. A., Quade, J., & Betancourt, J. L. (2002). Late Quaternary paleohydrology of the central
1036 Atacama Desert (lat 22°–24°S), Chile. *Bulletin of the Geological Society of America*,
1037 114(3), 334–348. [https://doi.org/10.1130/0016-7606\(2002\)114<0334:LQPOTC>2.0.CO;2](https://doi.org/10.1130/0016-7606(2002)114<0334:LQPOTC>2.0.CO;2)
- 1038 Rech, J. A., Pigati, J. S., Quade, J., & Betancourt, J. L. (2003). Re-evaluation of mid-Holocene
1039 deposits at Quebrada Puripica, northern Chile. In *Paleogeography, Paleoclimatology,*
1040 *Paleoecology* (Vol. 194, pp. 207–222). [https://doi.org/10.1016/S0031-0182\(03\)00278-5](https://doi.org/10.1016/S0031-0182(03)00278-5)
- 1041 Rech, J. A., Currie, B. S., Jordan, T. E., Riquelme, R., Lehmann, S. B., Kirk-Lawlor, N. E., ...
1042 Gooley, J. T. (2019). Massive middle Miocene gypsic paleosols in the Atacama Desert and
1043 the formation of the Central Andean rain-shadow. *Earth and Planetary Science Letters*,
1044 506, 184–194. <https://doi.org/10.1016/j.epsl.2018.10.040>
- 1045 Reutter, K. J., Charrier, R., Götze, H. J., Schurr, B., Wigger, P., Scheuber, E., ... & Chong, G.
1046 (2006). The Salar de Atacama Basin: a subsiding block within the western edge of the
1047 Altiplano-Puna Plateau. In *the Andes* (pp. 303–325). Springer Berlin Heidelberg.
- 1048 Risacher, F., Alonso, H., Salazar, C. (1999). *Geoquímica de aguas en cuencas cerradas: I, II y III*
1049 *Regiones–Chile. 1. Ministerio de Obras Públicas, pp. 209.*
- 1050 Risacher, F., Alonso, H., & Salazar, C. (2003). The origin of brines and salts in Chilean salars: a
1051 hydrochemical review. *Earth-Science Reviews*, 63(3), 249–293.
- 1052 Rissmann, C., Leybourne, M., Benn, C., & Christenson, B. (2015). The origin of solutes within
1053 the groundwaters of a high Andean aquifer. *Chemical Geology*, 396, 164–181.
1054 <https://doi.org/10.1016/j.chemgeo.2014.11.029>
- 1055 Rohrmann, A., Strecker, M. R., Bookhagen, B., Mulch, A., Sachse, D., Pingel, H., ... Montero,
1056 C. (2014). Can stable isotopes ride out the storms? The role of convection for water
1057 isotopes in models, records, and paleoaltimetry studies in the central Andes. *Earth and*
1058 *Planetary Science Letters*, 407, 187–195. <https://doi.org/10.1016/j.epsl.2014.09.021>
- 1059 Rosen, M. R. (1994). The importance of groundwater in playas: A review of playa classifications
1060 and the sedimentology and hydrology of playas. *Special Paper of the Geological Society*
1061 *of America*, 289, 1–18. <https://doi.org/10.1130/SPE289-p1>
- 1062 Sáez, A., Godfrey, L. V., Herrera, C., Chong, G., & Pueyo, J. J. (2016). Timing of wet episodes
1063 in Atacama Desert over the last 15 ka. *The Groundwater Discharge Deposits (GWD) from*
1064 *Domeyko Range at 25°S. Quaternary Science Reviews*, 145, 82–93.
1065 <https://doi.org/10.1016/j.quascirev.2016.05.036>
- 1066 Scanlon, B. R., Keese, K. E., Flint, A. L., Flint, L. E., Gaye, C. B., Edmunds, W. M., & Simmers,
1067 I. (2006). Global synthesis of groundwater recharge in semiarid and arid regions.
1068 *Hydrological Processes*, 20(15), 3335–3370. <https://doi.org/10.1002/hyp.6335>

- 1069 Scheihing, K. W., Moya, C. E., & Tröger, U. (2017). Insights into Andean slope hydrology:
 1070 reservoir characteristics of the thermal Pica spring system, Pampa del Tamarugal, northern
 1071 Chile. *Hydrogeology Journal*. <https://doi.org/10.1007/s10040-017-1533-0>.
- 1072 Skrzypek, G., Dogramaci, S., Rouillard, A., & Grierson, P. F. (2016). Groundwater seepage
 1073 controls salinity in a hydrologically terminal basin of semi-arid northwest Australia.
 1074 *Journal of Hydrology*, 542, 627–636. <https://doi.org/10.1016/j.jhydrol.2016.09.033>
- 1075 Stewart, M. K., Morgenstern, U., Gusyev, M. A., & Małoszewski, P. (2017). Aggregation effects
 1076 on tritium-based mean transit times and young water fractions in spatially heterogeneous
 1077 catchments and groundwater systems. *Hydrology and Earth System Sciences*, 21(9),
 1078 4615–4627. <https://doi.org/10.5194/hess-21-4615-2017>
- 1079 Stigter, E. E., Litt, M., Steiner, J. F., Bonekamp, P. N. J., Shea, J. M., Bierkens, M. F. P., &
 1080 Immerzeel, W. W. (2018). The Importance of Snow Sublimation on a Himalayan Glacier.
 1081 *Frontiers in Earth Science*, 6. <https://doi.org/10.3389/feart.2018.00108>
- 1082 Strecker, M. R., Alonso, R. N., Bookhagen, B., Carrapa, B., Hilley, G. E., Sobel, E. R., & Trauth,
 1083 M. H. (2007). Tectonics and Climate of the Southern Central Andes. *Annual Review of*
 1084 *Earth and Planetary Sciences*, 35(1), 747–787.
 1085 <https://doi.org/10.1146/annurev.earth.35.031306.140158>
- 1086 Tóth, J. (1963). A theoretical analysis of groundwater flow in small drainage basins. *Journal of*
 1087 *Geophysical Research*, 68(16), 4795–4812. <https://doi.org/10.1029/jz068i016p04795>
- 1088 Tsujimura, M., Abe, Y., Tanaka, T., Shimada, J., Higuchi, S., Yamanaka, T., ... Oyunbaatar, D.
 1089 (2007). Stable isotopic and geochemical characteristics of groundwater in Kherlen River
 1090 basin, a semi-arid region in eastern Mongolia. *Journal of Hydrology*, 333(1), 47–57.
 1091 <https://doi.org/10.1016/j.jhydrol.2006.07.026>
- 1092 Tyler, S.W., Kranz, S., Parlange, M.B., Albertson, J., Katul, G.G., Cochran, G.F., Lyles, B.A.,
 1093 Holder, G. (1997). Estimation of groundwater evaporation and salt flux from Owens Lake,
 1094 California, USA. *Journal Hydrology* 200, 110–135.
- 1095 Walvoord, M. A., Plummer, M. A., Phillips, F. M., & Wolfsberg, A. V. (2002). Deep arid system
 1096 hydrodynamics I. Equilibrium states and response times in thick desert vadose zones.
 1097 *Water Resources Research*, 38(12), 44-1-44–15. <https://doi.org/10.1029/2001WR000824>
- 1098 Ward, K. M., Zandt, G., Beck, S. L., Christensen, D. H., & McFarlin, H. (2014). Seismic imaging
 1099 of the magmatic underpinnings beneath the Altiplano-Puna volcanic complex from the
 1100 joint inversion of surface wave dispersion and receiver functions. *Earth and Planetary*
 1101 *Science Letters*, 404, 43–53. <https://doi.org/10.1016/j.epsl.2014.07.022>
- 1102 Ward, D. J., Cesta, J. M., Galewsky, J., & Sagredo, E. (2015). Late Pleistocene glaciations of the
 1103 arid subtropical Andes and new results from the Chajnantor Plateau, northern Chile.
 1104 *Quaternary Science Reviews*, 128, 98–116.
 1105 <https://doi.org/10.1016/j.quascirev.2015.09.022>
- 1106 WMC [Water Management Consultants Ltda.] (2007). Analisis de la relacion entre las aguas
 1107 subterranas del Proyecto Pampa Colorada, las vertientes y del margen este del Salar de
 1108 Atacama y las Lagunas Miscanti y Minique, Informe III Final, Santiago, Chile.
- 1109 Wheater, H., Sorooshian, S., & Sharma, K. D. (2007). Hydrological modelling in arid and semi-
 1110 arid areas. *Hydrological Modelling in Arid and Semi-Arid Areas* (Vol. 9780521869188,
 1111 pp. 1–212). Cambridge University Press. <https://doi.org/10.1017/CBO9780511535734>
- 1112 Wilson, J. L., & Guan, H. (2013). Mountain-Block Hydrology and Mountain-Front Recharge. In
 1113 *Groundwater Recharge in a Desert Environment: The Southwestern United States* (Vol. 9,
 1114 pp. 113–137). American Geophysical Union. <https://doi.org/10.1029/009WSA08>
- 1115 Wood, C., Cook, P. G., & Harrington, G. A. (2015). Vertical carbon-14 profiles for resolving
 1116 spatial variability in recharge in arid environments. *Journal of Hydrology*, 520, 134–142.
 1117 <https://doi.org/10.1016/j.jhydrol.2014.11.044>

- 1118 Van Beek, L.P.H., Wada, Y., Bierkens, M.F.P. (2011). Global monthly water stress: 1. Water
1119 balance and water availability. *Water Resources Research* 47, W07517.
1120 doi:10.1029/2010wr009791
- 1121 Vuille, M., & Ammann, C. (1997). Regional Snowfall Patterns in the High, Arid Andes. In
1122 *Climatic Change at High Elevation Sites* (pp. 181–191). Dordrecht: Springer Netherlands.
1123 https://doi.org/10.1007/978-94-015-8905-5_10
- 1124 Zimmerman, U., D. Ehhalt, and K.O. Munnich. (1967). Soil water movement and
1125 evapotranspiration: Changes in the isotopic composition of the water. Paper presented at
1126 International Atomic Energy Agency Symposium on Isotopes in Hydrology. Int. Atomic
1127 Energy Agency, Vienna, Austria.